1972

# Wind tunnel modeling of the atmospheric boundary layer

Sreemanth Pagadala



Department:

# WIND TUNNEL MODELING OF THE ATMOSPHERIC BOUNDARY LAYER

by

SREEMANTH PAGADALA, 1946-

---

A THESIS

Presented to the Faculty of the Graduate School of the

UNIVERSITY OF MISSOURI - ROLLA

In Partial Fulfillment of the Requirements for the Degree

MASTER OF SCIENCE IN MECHANICAL ENGINEERING

Rolla, Missouri

1972

Approved by

R. B. Oetting (Advisors) J. F. Stampfer

Daryl Akers

# ABSTRACT

The importance of simulating atmospheric flows in wind tunnels has been well established. Experiments were conducted in the Modified Aerodynamic Wind Tunnel to determine the suitability of this wind tunnel for simulating atmospheric flows and the degree to which various aspects of modeling could be fulfilled.

A temperature profile to simulate the inversion aloft was generated inside the test section, and then an appropriate velocity profile was built in by means of screen mesh arrangements. The turbulence characteristics of the flow were measured.

The validity of the temperature, velocity and turbulence fields were examined. It was found that while the temperature and velocity profiles were quite valid, the turbulence generated by the screen mesh arrangement was too high. The test section being short, turbulence could not be damped out to the required level.

A model smoke stack was introduced into the test section to observe the effect of the modeled inversion on the plume. The smoke velocity could not be effectively controlled, and the plume could only be observed a very short distance downstream. Therefore, the plume path was not very realistic. Other smoke tests in the test section showed maximum turbulence at the surface and no significant change when the temperature profile was introduced.

# ACKNOWLEDGEMENT

The author wishes to express his gratitude to his advisors, Dr. R.B. Oetting and Dr. J.F. Stampfer, Jr., for their efforts in guiding this thesis. The author is indebted to Dr. Oetting for the help and assistance on the wind tunnel and to Dr. Stampfer for suggesting and providing many helpful ideas on the modeling problems.

The author wishes to thank Dr. J. Podzimek for his helpful suggestions on designing the smoke generator, and D.W. Pepper for his assistance on the hot-wire instrumentation.

Gratitude is extended to the Department of Cloud Physics and the Office of Naval Research, who made this project possible under Themis grant N00014-68-A-0497.

# TABLE OF CONTENTS

Table of Contents Continued

# LIST OF ILLUSTRATIONS

List of Illustrations Continued

# LIST OF SYMBOLS

| | |
|---|---|
| $\alpha$, $\alpha'$ | Constant Associated with the Expression for Log-linear Law |
| $\beta$ | Constant Associated with Expression for Wind Profile |
| $c_v$ | Specific Heat of Air at Constant Volume |
| $c_p$ | Specific Heat of Air at Constant Pressure |
| $\gamma$ | Environmental Lapse Rate |
| $\Gamma$ | Adiabatic Lapse Rate |
| $\delta$ | Boundary Layer Height |
| e | Thermo-electric Power |
| E | EMF |
| F | Flux |
| Fr | Froude Number |
| g | Acceleration due to Gravity |
| H | Heat Flux |
| $\theta$ | Potential Temperature |
| k | von Karman's Constant |
| $\kappa$ | Ratio of Specific Heats |
| K | Eddy Diffusivity |
| $K_M$ | Eddy Diffusivity of Momentum |
| $K_H$ | Eddy Diffusivity of Heat |
| $\lambda$ | Any Characteristic Length |
| $\mu$ | Dynamic Viscosity of Air |
| L | Scale Length Associated with Similarity Law |
| $\upsilon$ | Kinematic Viscosity of Air |
| p | pressure of Air |
| $p_o$ | pressure at sea level |

List of Symbols Continued

| | |
|---|---|
| $\phi_m$ | Function Associated with Similarity Law |
| q | Constant Associated with Expression for Wind Profile |
| $R_m$ | Molecular Gas Constant |
| $\rho$, $\rho_a$ | Air Density |
| $\rho(z)$ | Density of Air at Height z |
| t | time |
| T | Temperature of Air |
| T(z) | Temperature of Air at Height z |
| $T_{ref}$ | Refererence Temperature |
| $\tau_o$ | Shear Stress at Surface |
| $\tau_z$ | Shear Stress at Height z |
| $u_*$ | Shear Velocity |
| $\bar{U}(z)$ | Mean Velocity at Height z |
| $\bar{U}_1$ | Reference Velocity Associated with Expression for Wind Profile |
| $\bar{U}$ | x Component of Mean Velocity |
| $\bar{V}$ | y Component of Mean Velocity |
| $\bar{W}$ | z Component of Mean Velocity |
| u' | x Component of Turbulence Intensity |
| v' | y Component of Turbulence Intensity |
| w' | z Component of Turbulence Intensity |
| x,z | Co-ordinate System |

# I. INTRODUCTION

The inversion layer of stably stratified air is a meteorological phenomena that has considerable influence on the diffusion and transport of particulate and gaseous effluents. Atmospheric motions being generally turbulent, the theoretical solutions, even in the statistical sense, are based on a high degree of empiricism. Experimental data of the actual phenomena are often expensive to obtain or inadequate. It therefore seems logical to model such flows on a reduced scale in wind tunnels.

Scale model experiments of the lower atmosphere have been conducted for many decades. The criteria for scale models of physical phenomena are being constantly improved and revised. The exact reproduction of a physical phenomena, especially in fluid flow, is very difficult, due to conflicting requirements. This therefore leads to compromise and corrections that normally result in a distorted model. The wind tunnel has long been recognized as a useful tool in modeling various problems related to aircraft flight and wind forces on man-made objects. Such a wind tunnel, due to its uniform air stream and constant velocity, is adequate for representing atmospheres at elevations far removed from the ground. It is possible to modify the wind tunnel to represent the non-uniform properties of the surface boundary layer. This modification will serve to enhance the use of the wind tunnel for

atmospheric simulation.

The non-uniform properties of the lower atmosphere are usually expressed in terms of the vertical profiles of mean velocity, turbulence and temperature. The region in which these occur is called the shear or boundary layer. Modeling starts with a reproduction of these properties to a suitable scale. In the atmosphere the horizontal component of wind is assumed to approach the geostrophic wind with an increase in height. This approach is such that there is a balance between the eddy stresses and the Coriolis stresses. In the laboratory boundary layer, the horizontal component of velocity approaches the free stream velocity such that there is a balance between the vertical eddy diffusion and the horizontal convection (SCHLICHTING, 1966). It has been pointed out by LUDWIG and SUNDARAM (1969), that the only portion of the planetary boundary layer that can be modeled by a laboratory boundary layer is that portion which does not depend explicitly on the geostrophic wind or the Coriolis parameter.

It has been emphasized that to have similitude is to have the same conservation equations and the same boundary conditions. Since the planetary boundary layer is described by different equations and boundary conditions from those of the laboratory flow generated by the existing methods, it is not possible to simulate the entire planetary boundary layer, but only the surface layer (LUDWIG and SUNDARAM, 1969).

There are two clearly defined methods for producing laboratory boundary layers of considerable thickness. The first method calls for a long test section in which the boundary layer is allowed to grow "naturally". The second requires a shorter test section and uses screens, vortex generators, etc. at the inlet to force the required profiles into the test section. CERMAK, et al (1965) used the first method in simulating atmospheric motions at the Colorado State University. LUDWIG and SUNDARAM (1969) used the second method at the Cornell Aeronautical Laboratory as has STROM (1966) at the New York University.

Stably stratified atmospheres modeled for surface inversions can be produced by controlling the surface temperatures as was done in the CSU wind tunnel. In atmospheric flows, a surface inversion causes most plumes rising through it to lose all their buoyancy and level off. This behaviour is called fanning. The fanning plume prevents diffusion vertically and as a result, the plume may not contact the ground until very far downwind. An inversion aloft on the other hand causes downward, but prevents upward, mixing and can therefore bring heavy concentrations of effluent to the ground nearer the source. This phenomenon is called fumigation. A need clearly exists for modeling this phenomena to assess its effect on particulate diffusion and transport.

The method used in this investigation was dictated by the size of the wind tunnel available. The experiments

were conducted in the UMR Horizontal Subsonic Wind Tunnel having a short test section. The wind tunnel is located in the Mechanical & Aerospace Engineering building.

# II. THEORETICAL BACKGROUND

## A. Thermal Structure of the Atmosphere

The temperature of the air below the stratosphere decreases, on the average, with an increase in altitude. The actual gradient of the temperature of the atmosphere with height is called the environmental lapse rate, $\gamma$, and is given by

$$\gamma = - \frac{dT}{dz} \tag{2-1}$$

where T is the absolute temperature and z the height. The dry adiabatic lapse rate, $\Gamma$, on the other hand, is numerically equivalent to that temperature change a parcel of dry air would undergo if lifted vertically and adiabatically. It is given by

$$\Gamma = - \frac{dT}{dz} = \frac{g}{c_p} \tag{2-2}$$

where g is the acceleration due to gravity and $c_p$ the specific heat of air at constant pressure. From equation (2-1), if $T(z_1)$ is the temperature at height $z_1$ and $T(z_2)$ the temperature at height $z_2$

$$T(z_2) = T(z_1) - \gamma \, \Delta z \tag{2-3}$$

where $\Delta z = (z_2 - z_1)$. If the environmental lapse rate is equal to the adiabatic lapse rate then

$$T(z_2) = T(z_1) - \Gamma \Delta z \tag{2-4}$$

In an atmosphere possessing such a temperature distribution a parcel of air moved adiabatically from one level to another will always have the same density as the surrounding air.

The definition of potential temperature of dry air, $\theta$, is the temperature which a volume of air assumes when brought adiabatically from its existing pressure to a pressure of 1000 mb, and is given by

$$\theta = T\left[\frac{p_o}{p}\right]^{\frac{\kappa-1}{\kappa}} \tag{2-5}$$

where $p_o$ is 1000 mb, and $\kappa$ is the ratio of the specific heat at constant pressure to that at constant volume. The gradient of potential temperature may be expressed in terms of the gradient of (absolute) temperature T and the adiabatic lapse rate $\Gamma$. Differentiating equation (2-5) in its logarithmic form gives

$$\frac{d(\ln\theta)}{dz} = \frac{d}{dz}\left(\ln T - \frac{\kappa-1}{\kappa}\ln\frac{p}{p_o}\right) \tag{2-6}$$

or

$$\frac{1}{\theta}\frac{d\theta}{dz} = \frac{1}{T}\frac{dT}{dz} - \frac{\kappa-1}{\kappa}\frac{1}{p}\frac{dp}{dz} \tag{2-7}$$

Substitution of the hydrostatic equation, $\frac{dp}{dz} = -g\rho$, into

equation (2-7) results in

$$\frac{1}{\theta}\frac{d\theta}{dz} = \frac{1}{T}\frac{dT}{dz} + \frac{\kappa-1}{\kappa}\frac{1}{p}g\rho \qquad (2\text{-}8)$$

Noting that

$$\frac{\kappa-1}{\kappa} = \frac{c_p - c_v}{c_p} = \frac{R_m}{c_p} \qquad (2\text{-}9)$$

where $c_v$ is the specific heat at constant volume and $R_m$ is the molecular gas constant for dry air, substituting this relation into equation (2-8), yields

$$\frac{1}{\theta}\frac{d\theta}{dz} = \frac{1}{T}\frac{dT}{dz} + \frac{\rho}{p}\frac{g}{c_p}R_m \qquad (2\text{-}10)$$

Making use of the equation for the dry adiabatic lapse rate (2-2) and the equation of state for an ideal gas

$$p = \rho R_m T \qquad (2\text{-}11)$$

equation (2-10) becomes

$$\frac{1}{\theta}\frac{d\theta}{dz} = \frac{1}{T}\left[\frac{dT}{dz} + \Gamma\right] \qquad (2\text{-}12)$$

The term S, which shall be called the stability, is given by

$$S = \frac{dT}{dz} + \Gamma = -\gamma + \Gamma \qquad (2\text{-}13)$$

and is the difference between the existing or environmental

gradient of temperature and the adiabatic lapse rate. It is a measure of the static stability of the atmosphere. If $S>0$, then the potential temperature increases with height, and a statically stable atmosphere exists. If $S<0$, the potential temperature decreases with an increase in height and an unstable atmosphere results. If $S=0$, the potential temperature remains constant and the atmosphere is neutrally stable. The dry adiabatic lapse rate is numerically equal to $9.86^{\circ}C$ per Km.

When the actual temperature decreases faster with height than the adiabatic rate, $\gamma>\Gamma$, the lapse rate is termed superadiabatic. A rising parcel of air, cooling at the adiabatic rate, becomes warmer and less dense than its environment and therefore buoyancy tends to accelerate it upwards. Such a parcel of air is in unstable equilibrium. When the environmental lapse rate is less than adiabatic, $\gamma<\Gamma$, it is called subadiabatic and a rising air parcel becomes cooler and more dense than its environment and tends to return to its initial point. Such a parcel of air is in stable equilibrium. As instability and stability are defined with reference to a neutral equilibrium represented by the dry adiabatic lapse rate for dry or unsaturated air, environmental lapse rates in stable layers may have positive, zero or negative values. The lapse rate in an isothermal layer is zero. The lapse rate is negative when the temperature increases with height and the condition is termed an inversion, while lapse rates between $\Gamma$ and 0 are

termed subadiabatic. Figure (2-1) illustrates the various lapse rates and indicates their stability.

Figure (2-2) shows the formation of different temperature profiles. The diurnal variation of temperature in the lowest layers of the atmosphere is a common place feature of daily life. During the hours of daylight, from shortly after dawn to about an hour before sunset, temperature usually decreases with height, rapidly in the lowest layers and more slowly at the greater heights. With the setting in of dusk, radiative cooling of the ground and exchange of heat between the ground and the lowest layers starts the mechanism for the formation of a surface inversion which grows in height. At dawn, the radiative heating from the sun breaks up the inversion in the lowest layers and an inversion aloft is formed. This inversion is often a temporary feature and may be destroyed with further radiative heating and subsequent convective mixing. Inversions aloft may also be due to overriding of warm air masses, as at frontal surfaces, subsidence of air masses, and radiation from the tops of clouds or fog (WANTA, 1968).

## B. Wind Structure of the Surface Boundary Layer

For most purposes in meteorology, the atmosphere is regarded as incompressible. The estimation of velocity at altitude is based on the assumption that the air adjusts its speed to maintain a balance involving only the pressure gradient and the forces arising from the rotation of the

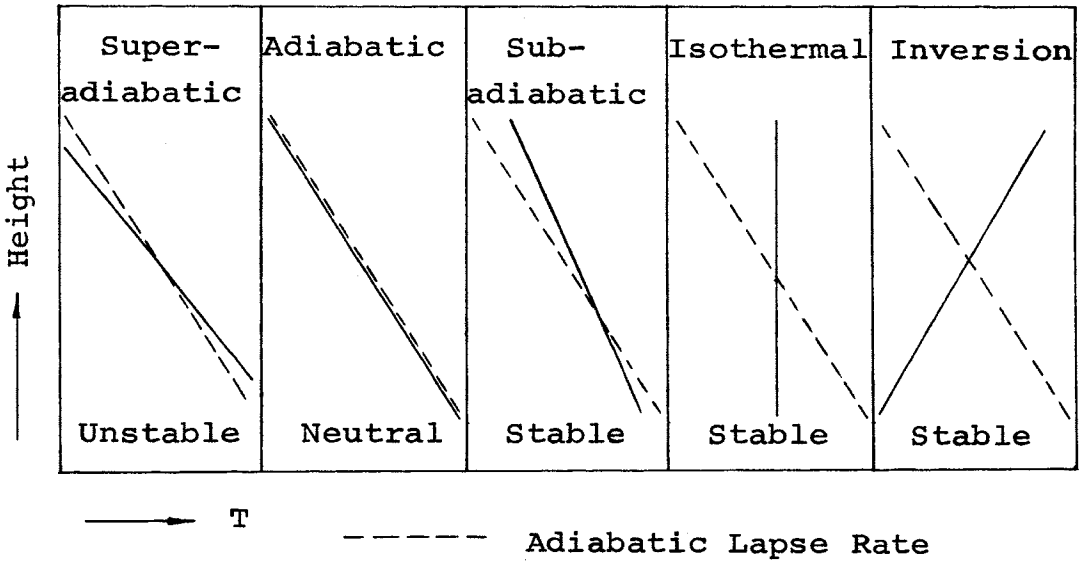


Figure 2-1. Various Types of Lapse Rates

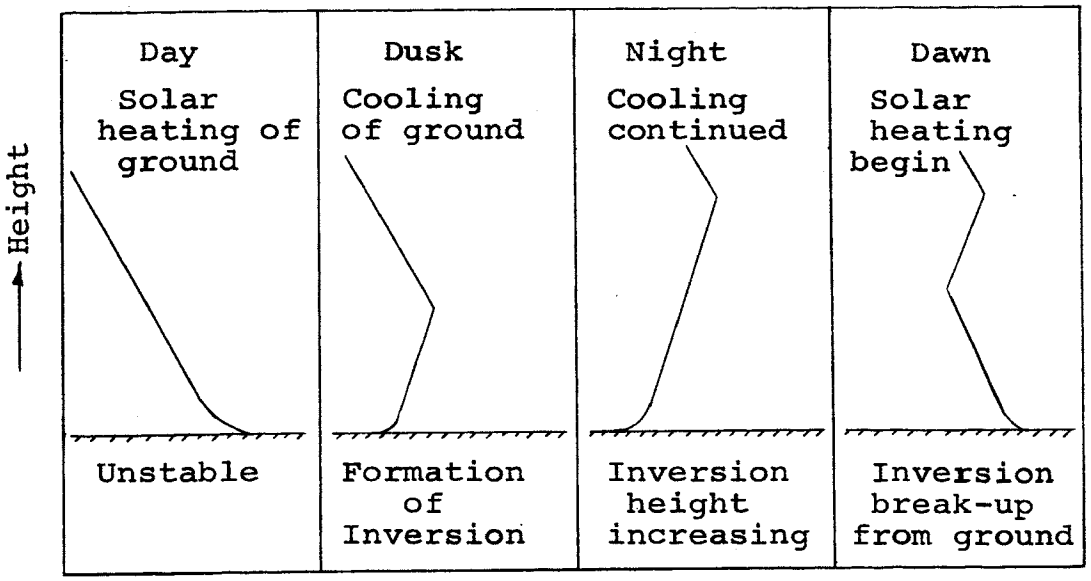


Figure 2-2. Formation of Temperature Profiles

earth. This velocity is known as the geostrophic wind and is a useful approximation of the actual wind speed at heights normally above 500 or 1000 meters. In problems involving wind very near the surface, it is usually possible to treat the pressure gradient as a constant driving force and to ignore entirely the effects of the Coriolis force. SUTTON (1953) considers the atmosphere to be divided into horizontal layers. In the surface boundary layer, extending to not more than 100 meters above the surface, the effects of the earth's rotation may be disregarded in comparison with effects which arise from the surface itself. Enveloping the surface layer, and extending to about one kilometer above the surface is the deeper friction layer, or planetary boundary layer, a zone of transition from the disturbed flow near the surface to the smooth frictionless flow of the free atmosphere. The problem of wind structure in this layer involves not only the pressure gradient and the Coriolis force but also the residual frictional effects of the earth's surface.

1. Wind Profiles, Stability and Mixing

From studies of wind profiles in the surface boundary layer, early investigators expressed the velocity profile in the form

$$\bar{U} = \bar{U}_1 z^q \qquad (2\text{-}14)$$

where q was greater than zero and was a function of the

stability, $\bar{U}$ the velocity at height z, and $\bar{U}_1$ a reference velocity. SUTTON (1953) showed that the index q in equation (2-14) varied from a value of 1/6 for inversions to about 1/14 for superadiabatic conditions. Other investigators arrived at a value of 1/7 for q under neutral conditions. A similar profile was obtained with a flat plate turbulent boundary layer flow and was known as the "seventh root law" (SCHLICHTING, 1966). DEACON (1949) and LAIKHTMAN (1944) proposed the following relation for the wind profile

$$\frac{d\bar{U}}{dz} = a\, z^{-\beta} \qquad (2\text{-}15)$$

where 'a' is a constant and independent of height, and $\beta$ is greater or less than unity in unstable or stable conditions, respectively. However, for small deviations from the adiabatic lapse rate, $\beta$ approaches 1. DEACON'S observation showed that $\beta$ was not completely independent of height. Taking the roughness of the surface into consideration SUTTON gave expressions for wind velocity in the surface boundary layer for neutral conditions.

Smooth flow:
$$\frac{\bar{U}}{u_*} = \frac{1}{k} \ln\left(\frac{u_* z}{\upsilon}\right) + 5.5 \qquad (2\text{-}16)$$

Rough flow:
$$\frac{\bar{U}}{u_*} = \frac{1}{k} \ln\left[\frac{z}{z_o}\right] \qquad (2\text{-}17)$$

where k is the von Karman constant ($\simeq 0.41$), $z_o$ the

roughness length, $\upsilon$ the kinematic viscosity and $u_*$ the friction velocity defined as

$$u_* = \sqrt{(\tau_o/\rho)} \tag{2-18}$$

where $\tau_o$ is the shear stress at the surface.

The "similarity theory" of MONIN & OBUKHOV (1954) has provided a fundamental framework for determining the relation between wind and temperature distribution in the surface boundary layer based on the log-linear velocity law given by equation (2-17). MONIN & OBUKHOV in their similarity theory relate various dimensionless variables to the dimensionless height ratio z/L, where the scale length L is defined by

$$L = - \frac{u_*^3 \; c_p \; \rho \; T}{k \; g \; H} \tag{2-19}$$

where H is the vertical heat flux (positive upwards). The gradient of velocity in the non-dimensional form (PLATE, 1971) is given by

$$\frac{k \; z}{u_*} \frac{d\bar{U}}{dz} = \phi_m(z/L) \tag{2-20}$$

and expanding the function $\phi_m$ about a Taylor's series and truncating the series after the first two terms, equation (2-20) becomes

$$\frac{d\bar{U}}{dz} = \frac{u_*}{k \; z} \left[ 1 + \alpha \; \frac{z}{L} \right] \tag{2-21}$$

where $\alpha$ is a numerical constant to be determined from observations. The integrated form of equation (2-21) is

$$\bar{U} = \frac{u_*}{k}\left[\ln\frac{z}{z_o} + \alpha\,\frac{z}{L}\right] \qquad (2\text{-}22)$$

where the velocity $\bar{U}$ is zero at $z = z_o$ and $z_o$ is small compared with z. Equation (2-22) gives the velocity as a function of height in the log-linear form with the correction term depending linearly on z/L. WEBB (1969) obtained a value of 4.5 for $\alpha$ in unstable conditions and 5.2 in stable conditions. Other researchers have arrived at different values and PLATE (1971) has concluded that the value of $\alpha$ depends on the range of z/L.

Since the ratio z/L in equation (2-22) can be measured only if the vertical heat flux is known, which is rarely the case, the temperature and wind velocity gradients are used to obtain z/L in the following manner.

The flux, F, of a given property, $\bar{s}$, across a fixed surface is given by

$$F = -\,\rho\,K\,\frac{\partial \bar{s}}{\partial n} \qquad (2\text{-}23)$$

where $\rho$ is the density of the medium, air in this case, $\frac{\partial \bar{s}}{\partial n}$ is the gradient perpendicular to the surface and K is the eddy diffusivity. From the definition of eddy diffusivity then

$$K_M = \frac{\tau_z}{\rho}\,\frac{1}{(\partial \bar{U}/\partial z)} \qquad (2\text{-}24)$$

where $K_M$ is eddy diffusivity of momentum. The constancy of shearing stress with height in the lower atmosphere (as also of the vertical flux of water vapor) is now accepted as a general principle (PASQUILL, 1962). Therefore

$$\frac{\tau_z}{\rho} = \frac{\tau_o}{\rho} = u_*^2 \qquad (2\text{-}25)$$

Substituting equation (2-25) in equation (2-24), the eddy diffusivity in terms of the friction velocity $u_*$ is

$$K_M = \frac{u_*^2}{(\partial \bar{U}/\partial z)} \qquad (2\text{-}26)$$

The eddy diffusivity for heat, $K_H$, is derived in a similar manner as

$$K_H = - \frac{H}{c_p \rho \, (\partial \theta/\partial z)} \qquad (2\text{-}27)$$

Equation (2-19) is used to determine z/L in the form

$$\frac{z}{L} = - \frac{z \, k \, g \, H}{u_*^3 \, c_p \, \rho \, T} \qquad (2\text{-}28)$$

Solving equations (2-26) and (2-27) for $u_*$ and $\frac{H}{c_p \rho}$, respectively, and substituting these values into equation (2-28) yields

$$\frac{z}{L} = \frac{K_H}{K_M} \frac{g}{T} \frac{(\partial \theta/\partial z)}{(\partial \bar{U}/\partial z)} \frac{1}{(u_*/k \, z)} \qquad (2\text{-}29)$$

Assuming $K_H = K_M$

$$\frac{z}{L} = \frac{g}{T} \frac{(\partial\theta/\partial z)}{(\partial\bar{U}/\partial z)} \frac{1}{(u_*/k\ z)} \tag{2-30}$$

From equation (2-21)

$$\frac{u_*}{k\ z} = \frac{d\bar{U}}{dz} \left[ 1 + \alpha \frac{z}{L} \right]^{-1} \tag{2-31}$$

and substituting this into equation (2-30) yields

$$\frac{z}{L} = \frac{g}{T} \frac{(\partial\theta/\partial z)}{(\partial\bar{U}/\partial z)^2} \left[ 1 + \alpha \frac{z}{L} \right] \tag{2-32}$$

Equation (2-32) can be written as

$$\frac{z}{L} = \frac{Ri}{(1 - \alpha\ Ri)} \tag{2-33}$$

where

$$Ri = \frac{g}{T} \frac{(\partial\theta/\partial z)}{(\partial\bar{U}/\partial z)^2} \tag{2-34}$$

is the gradient Richardson number. The Richardson number provides a criteria for classifying flows according to their stability. In the atmosphere measurements seem to indicate that turbulence is not found above a value of about Ri = +0.2 (BLACKADAR, 1960). BATCHELOR (1953) has shown that in stratified flow close to the ground dynamic similarity depends entirely on the Richardson number.

If however the ratio $K_H/K_M$ is not unity then

$$\frac{z}{L'} = \frac{Ri}{(1 - \alpha' Ri)} \qquad (2\text{-}35)$$

where $L' = L(K_H/K_M)$ and $\alpha' = \alpha(K_H/K_M)$. WEBB (1969) has shown that the log-linear profile for wind is valid in stable air, not only for small z/L' but for z/L' up to 0.3. The corresponding Richardson number was 0.1. When z/L' exceeds the value of 0.3, it has been shown that no simple wind profile fits the flow (LUMLEY & PANOFSKY, 1964). In the range of Richardson number from 0 to 0.08 McVEHIL (1962) does not find any systematic difference between $K_H$ and $K_M$. For very large Richardson numbers, $K_H$ falls off more rapidly with height than $K_M$.

2. Shear Stress Characteristics of Flows

It is necessary to explore the compatibility between the variation of shear stress with height in atmospheric boundary layer flow to that in the artificially produced boundary layer in the laboratory. In atmospheric surface layer theories it is assumed that the shear stress does not vary with height. This assumption is used to obtain the logarithmic velocity law, equation (2-16).

Considering the momentum equation, in the flow direction, for the general case

$$\frac{\partial \bar{U}}{\partial t} + \bar{U}\frac{\partial \bar{U}}{\partial x} + \bar{V}\frac{\partial \bar{U}}{\partial y} + \bar{W}\frac{\partial \bar{U}}{\partial z} = f\bar{U} - \frac{1}{\rho}\frac{\partial p}{\partial x} + \frac{\partial \sigma_x}{\partial x} + \frac{\partial \tau_{xy}}{\partial y} + \frac{\partial \tau_{xz}}{\partial z} \qquad (2\text{-}36)$$

where $\bar{U}$, $\bar{V}$ and $\bar{W}$ are the components of velocity in the x, y and z directions, respectively, and

$$\begin{aligned} \sigma_x &= - \rho \, \overline{u'^2} \\ \tau_{xy} &= - \rho \, \overline{u'v'} \\ \tau_{xz} &= - \rho \, \overline{u'w'} \end{aligned} \qquad (2\text{-}37)$$

with u', v' and w' the turbulence intensities in the x, y and z directions, respectively, and $f\bar{U}$ the Coriolis force. Considering an ideal situation in which all conditions are steady, and the velocity and turbulence are horizontally homogeneous, equation (2-36) reduces to

$$f\bar{U} - \frac{1}{\rho} \frac{\partial p}{\partial x} - \frac{1}{\rho} \frac{\partial \tau_{xz}}{\partial z} = 0 \qquad (2\text{-}38)$$

ELLISON (1956) has shown that this equation is valid within the planetary boundary layer. In the surface layer where the Coriolis force is considered negligible, equation (2-38) reduces to

$$\frac{d\tau_{xz}}{dz} = - \frac{\partial p}{\partial x} \qquad (2\text{-}39)$$

Equation (2-39) shows that the variation of shear stress with height in the surface boundary layer is dependent on the pressure gradient in the direction of the flow. Pressure gradients encountered in the atmosphere are very small and subsequently the shear stress is taken as constant

with height. In the wind tunnel equation (2-39) is valid. However, the pressure gradients are relatively larger than those in the atmosphere and will therefore not produce the constant shear stress required to simulate atmospheric flow.

One way to reduce pressure gradients along the flow in the wind tunnel is to adjust the roof of the test section so that there is a gradual increase in area. Even by decreasing the pressure gradients, the shear stress will not be constant throughout the height of the test section. Therefore, the height to which the shear stress remains fairly constant is usually taken as the height of the model boundary layer.

## C. Modeling Criteria

STROM (1969) has used dimensional analysis for the formulation of modeling factors for simulation of atmospheric motions. The number of variables and the complexity of atmospheric flows makes the application of analytical procedures tedious and usually produces a mathematically cumbersome solution. Most analytical systems developed for atmospheric flows are either inaccurate or incomplete. Therefore, dimensional analysis supplemented by experimental evidence may lead to the enunciation of a general law governing the phenomenon under consideration.

### 1. Determination of Non-dimensional Pi Terms

Consider a parcel of air released suddenly into the

atmosphere inside the region of the surface boundary layer. If the problem is assumed two dimensional, ie., in the x and z plane (where x is along the mean flow direction and z perpendicular to it), and the air parcel has at time t = 0 ordinates (0,0), then coordinates of the air parcel from its reference coordinate is given by

$$z_a, x_a = f(\lambda, \delta, \bar{U}(z), \bar{U}_o, d\bar{U}/dz, \rho_a, \rho(z), \Delta(d\rho/dz), g, \mu, \kappa) \quad (2\text{-}40)$$

where

$x_a$ = distance along the x axis in the direction of mean flow

$z_a$ = vertical distance along the z axis

$\lambda$ = any characteristic length in the x or z direction

$\delta$ = surface boundary layer thickness

$\bar{U}(z)$ = mean velocity at height z inside the surface boundary layer

$\bar{U}_o$ = mean velocity at height $\delta$

$d\bar{U}/dz$ = mean velocity gradient in the surface boundary layer

$\rho_a$ = density of the air parcel released

$\rho(z)$ = density of air at height 'z' within the surface boundary layer

$\Delta(d\rho/dz)$ = difference between actual density gradient and adiabatic density gradient

$g$ = acceleration due to gravity

$\kappa$ = ratio of specific heats, $c_p$ to $c_v$

$\mu$ = dynamic viscosity of air.

By dimensional analysis the following is obtained

$$\frac{z_a}{\delta}, \frac{x_a}{\delta} = f\left\{\frac{\lambda}{\delta}, \frac{\bar{U}(z)}{\bar{U}_o}, \frac{\delta}{g}(d\bar{U}/dz)^2, \frac{\delta\Delta(d\rho/dz)}{\rho}, \frac{\rho\bar{U}_o\delta}{\mu}, \frac{\rho}{\rho_a}, \frac{\rho\bar{U}_o^2}{\Delta\rho g\delta}\right\} \tag{2-41}$$

The dimensionless ratios on the right are scale factors which should be maintained at the same values in model and prototype. The ratios of dependent variables on the left and the first dimensionless term on the right indicate that geometric similarity should exist throughout the physical model. The second term indicates that the similarity of velocity profiles should be preserved. The third and fourth factors determine the velocity and density profiles.

For the velocity profile

$$\frac{\delta}{g}\left[\frac{d\bar{U}}{dz}\right]^2_{\text{atm.}} = \frac{\delta}{g}\left[\frac{d\bar{U}}{dz}\right]^2_{\text{model}} \tag{2-42}$$

and for the density profile,

$$\frac{\delta}{\rho}\Delta\left[\frac{d\rho}{dz}\right]_{\text{atm.}} = \frac{\delta}{\rho}\Delta\left[\frac{d\rho}{dz}\right]_{\text{model}} \tag{2-43}$$

The value of $\rho$ from the equation of state is substituted into equation (2-43). The resulting equation is

differentiated and using the hydrostatic equation one obtains

$$\frac{\delta}{T}\left[\frac{dT}{dz} + \Gamma\right]_{atm.} = \frac{\delta}{T}\left[\frac{dT}{dz} + \Gamma\right]_{model} \qquad (2\text{-}44)$$

which may be written as

$$\frac{\delta}{T}\left[\frac{d\theta}{dz}\right]_{atm.} = \frac{\delta}{T}\left[\frac{d\theta}{dz}\right]_{model} \qquad (2\text{-}45)$$

Dividing equation (2-45) by equation (2-42) gives

$$\frac{g}{T}\left\{\frac{(d\theta/dz)}{(dU/dz)^2}\right\}_{atm.} = \frac{g}{T}\left\{\frac{(d\theta/dz)}{(dU/dz)^2}\right\}_{model} \qquad (2\text{-}46)$$

which is by definition the Richardson number. Equation (2-46) shows the necessity of the equality of the Richardson numbers in the atmospheric surface layer and the model boundary layer.

The fifth factor is the Reynolds number which should theoretically be the same for the model and atmosphere. It is found, however, that if the flow is aerodynamically rough and inertia forces do not dominate, then the Reynolds number is of little importance (STROM, 1966).

The sixth factor shows that the ratios of the densities of air in the surface boundary layer should be the same as those in the model boundary layer. Instead of a theoretical parcel of air, it is usual to consider the density of a plume in the ratio of densities requirement.

The last factor is the square of the Froude number

$$Fr^2 = \left[\frac{\rho\ \bar{U}_o^2}{\Delta\rho\ g\ \delta}\right]_{atm.} = \left[\frac{\rho\ \bar{U}_o^2}{\Delta\rho\ g\ \delta}\right]_{model} \qquad (2\text{-}47)$$

where $\Delta\rho$ is the difference in density between the plume and air. It is impossible to satisfy both the Froude and Reynolds number criteria simultaneously. However, as already stated, Reynolds number is of little importance. Further, buoyant gas plumes have an unrealistic plume path if the Froude number criterion is not maintained. Thus, the emphasis in the modeling is on the Froude number rather than the Reynolds number. There are no variables in the above analysis for inclusion of turbulence effects. Turbulence variables are implicit in the velocity profile requirement $\bar{U}(z)/\bar{U}_o$, since the profile is dependent on the turbulent shear stress.

In summary, it can be stated that similarity in velocity and temperature profiles is to be preserved. The flow should be aerodynamically rough, so as to ignore the Reynolds number criteria. The Richardson numbers should be the same for model and atmosphere for corresponding layers in the flow.

2. Choice of Scale Length

Usually the scale length of modeling is determined by the height of the boundary layer developed in the wind tunnel which is again dictated by the cross sectional size of the test section. When the boundary layer height is

defined as the height where the velocity reaches 99 per cent of the free stream velocity, an exact height is difficult to determine. Another method is to use direct geometric scaling as in the use of roughness elements to simulate a rough ground in atmospheric flows. A common method to determine the scale length is based on the criteria that the shear stress should remain constant with height. Here, the wind tunnel flow produces only a limited height of constant shear stress due to the pressure gradients along the flow. The height of the boundary layer is taken as the height to which the constant shear layer extends from the surface of the model flow. A choice of a certain scale length has to satisfy both the velocity and temperature modeling criteria. A very large scaling factor when used to adjust temperature gradients to values required in the atmosphere will upset the velocity requirements. In scaling, the temperature varies as the scale factor but the velocity varies as the square root of the scale factor. This presents a problem, as very large velocities will result for the atmospheric values when large scaling factors are used. All these criteria have to be considered when making a choice of the scaling length. Other means of selecting scale factors include: i. the Monin-Obhukov scale length; ii. the mixing length criteria; and iii. Reynolds number criteria. This last method is used for flows that develop boundary layers by natural growth.

# III. EXPERIMENTAL EQUIPMENT

The experimental equipment consists of the modified aerodynamic horizontal wind tunnel, wire mesh screens, splitter plate and heating element, a smoke generating apparatus, and a series of instruments for velocity, turbulence and temperature measurements.

## A. The Modified Aerodynamic Horizontal Wind Tunnel

The wind tunnel is of the open circuit type, with intake air coming from within the laboratory. The wind tunnel, shown in Figure (3-1), is housed in the first floor open laboratory of the Mechanical and Aerospace Engineering building. Air is drawn through the wind tunnel by a centrifugal flow fan located at the end of the diffuser section. The fan speed range is from 1800 RPM to 2000 RPM, the 10 per cent speed range control being provided by controlling the current through a rheostat on the instrument panel of the 20 HP fan drive motor. A wider range in velocity is obtained by controlling the exhaust air flow at two points, viz., at the exhaust port of the centrifugal fan by means of a "bread board", pushed in to limit flow and pulled out to increase the flow; and at the end of the exhaust ducting by varying the orifice size. A combination of the motor speed and the exhaust flow controls gives a velocity range from a maximum of 80 feet per second to as low as a few feet per second in the test section.

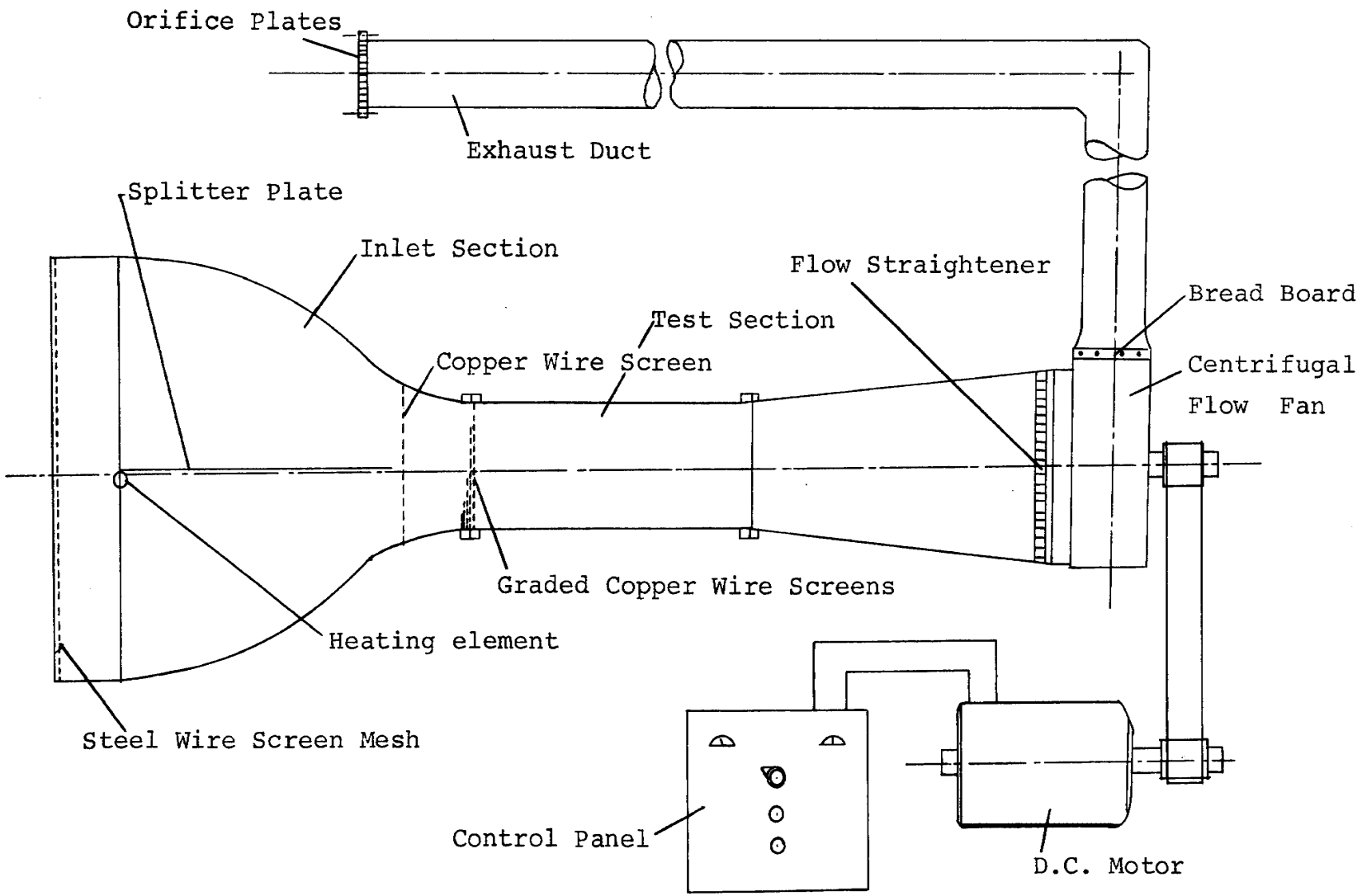


Figure 3-1. Modified Horizontal Aerodynamic Wind Tunnel

The contraction ratio of the inlet section is 7.3 to 1.0. The inlet section is provided with the following:

1. Wire mesh screen (steel wire), 18 squares to the inch and 0.018 inch wire diameter, is stretched across the entrance of the inlet section to ensure horizontal intake of air.

2. One tubular heating element, 3/8 inch diameter and 56 inches long is placed horizontally across the middle of the inlet section entrance. The heating element provides the required temperature profile in the test section. A maximum temperature of 350$^{o}$C can be attained at the surface of the heating element. The temperature of the element is controlled by a proportional controller which draws its power from a 220 volt, 3 phase supply.

3. A horizontal splitter plate made of aluminum and conforming to the shape of the inlet section is located along the inlet center line to reduce the convective motions of hot air masses at the low velocities encountered in the inlet section. The plate extends from the beginning of the inlet section to 2 feet before the entrance of the test section.

4. Wire mesh screen (copper wire), 18 squares to the inch and wire diameter 0.016 inch is located at the downstream end of the splitter plate to redistribute evenly the divided velocities produced by the splitter plate.

5. Wire mesh screens (copper wire) with the same gauge as in 4, of different heights (5, 9, 14 and 20 inches

from the bottom) and the same width (20 inches) are lapped together and located at the entrance of the test section to generate the required velocity profile. In addition to these screens there is also a 2 inch high masking tape fence placed at the bottom of the test section entrance to trip the boundary layer. This method of generating a velocity profile by means of wire mesh screens is due to LLOYD (1969), who suggested the use of horizontal rows of round bars, grids or graded mesh screens to generate velocity profiles.

The test section of the wind tunnel is 20 inches square and 42 inches long in the direction of the mean flow. Two plexiglass sheets, one of 0.25 inch thickness and the other of 0.50 inch thickness form the back and front of the test section, respectively, and are mounted by means of bolts and wing nuts.

The end of the diffuser is fitted with an "egg crate" flow straightener made of 1 inch deep (in the direction of flow) tin sheets and forming 1 inch square holes.

B. The Smoke Generating Apparatus

Figure (3-2) shows the smoke generator. The generator consists of a cylindrical pyrex glass jar, in which a ceramic tube wrapped with fibre glass heating tape and filled with fibre glass wool stands vertically. The space between the ceramic tube and the jar is also filled with fibre glass wool. Two flat aluminum plates are bolted

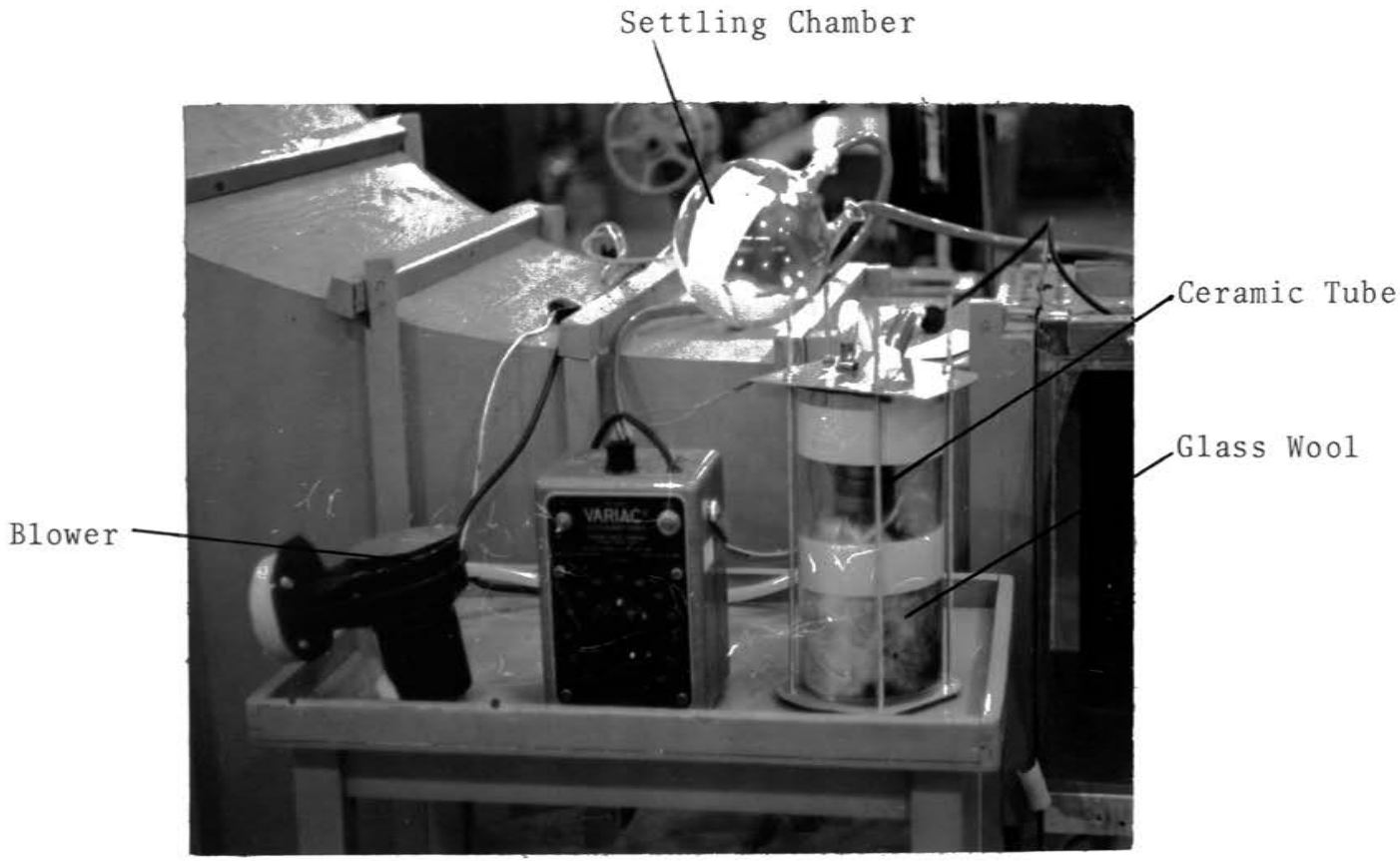


Figure 3-2. The Smoke Generator

together sandwiching the top and bottom of the glass jar between them. The upper plate has three taps, one for the delivery of kerosene, one for blowing air into the jar and the third for transporting the smoke out of the system. A rubber gasket is used between the glass jar and the top plate to prevent leakage. Kerosene from a drip tube falls on the heated ceramic tube or the glass wool on its inside. A 0.5 HP blower generates enough pressure to displace the generated smoke from the glass jar out through the exit tap and into a settling chamber. The nearly dry, cooled smoke is then blown into the test section.

C. Instrumentation

Similitude requirements for atmospheric flow processes are met if mean velocities, turbulence intensities and temperatures are reproduced to an adequate scale. The instruments used for measuring these quantities are as follows:

1. Temperature Measurements

Temperature differences between a reference point and other points at different heights of the test section are measured by means of two copper-constantan thermocouples. A reference thermocouple is taped 0.5 inch above the floor of the test section. The other thermocouple is attached to the traversing mechanism which will be described later. The location of the reference thermocouple at the bottom of the test section is to provide a region of constant

temperature. This region is removed from the effects of heating which is felt only 8 inches from the bottom of the test section. The difference in temperature recorded by the two thermocouples is given by

$$T_a - T_{ref.} = \frac{E}{e} \qquad (3\text{-}1)$$

where $T_a$ is the temperature at the measuring thermocouple and $T_{ref.}$ is the temperature at the reference thermocouple. E is the EMF corresponding to the voltmeter deflection and e is the thermoelectric power in microvolts per degree Centigrade. For a temperature range from $0^{o}C$ to $100^{o}C$, e for a copper-constantan thermocouple is 40 μV per $^{o}C$. The generated EMF is read with a KEITHLEY, 149 milli-micro voltmeter shown in Figure (3-3).

2. Velocity and Turbulence Measurements

Mean velocity and turbulent fluctuations are measured by hot wire anemometry. Figure (3-3) shows the hot wire instrumentation. A complete description of the use, calibration and measurement with the hot wire anemometer can be found in the thesis by PEPPER (1970).

3. The Traversing Mechanism

A 0.75 inch diameter lead screw 24 inches long and with 11 threads to the inch is used as the rotating component of the traversing mechanism. It passes through a hole in the ceiling of the test section, and stands vertically, supported at the floor by a teflon bearing.

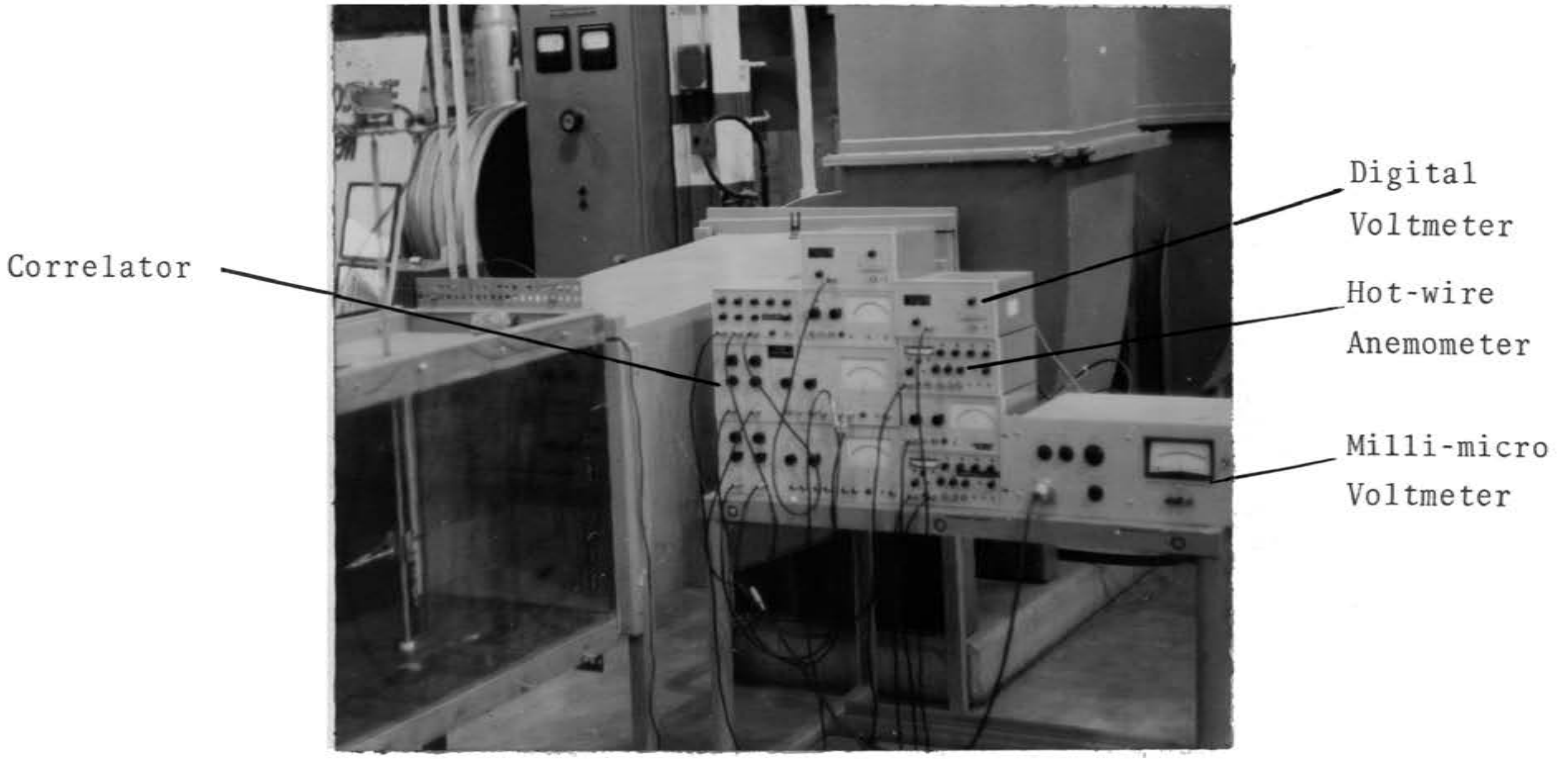


Figure 3-3. Hot-wire and Temperature Instrumentation

A nut on to which is clamped an aluminum bracket traverses the height of the test section when the lead screw is rotated. The rotary motion is produced by means of a 0.25 HP reversing motor coupled to the top of the lead screw. The aluminum bracket is prevented from rotating by a constraining steel rod, 0.5 inch in diameter, and fixed parallel to the lead screw inside the test section. The measuring thermocouple and hot wire probe holders are mounted on the aluminum bracket. Figure (3-4) shows the traversing mechanism.

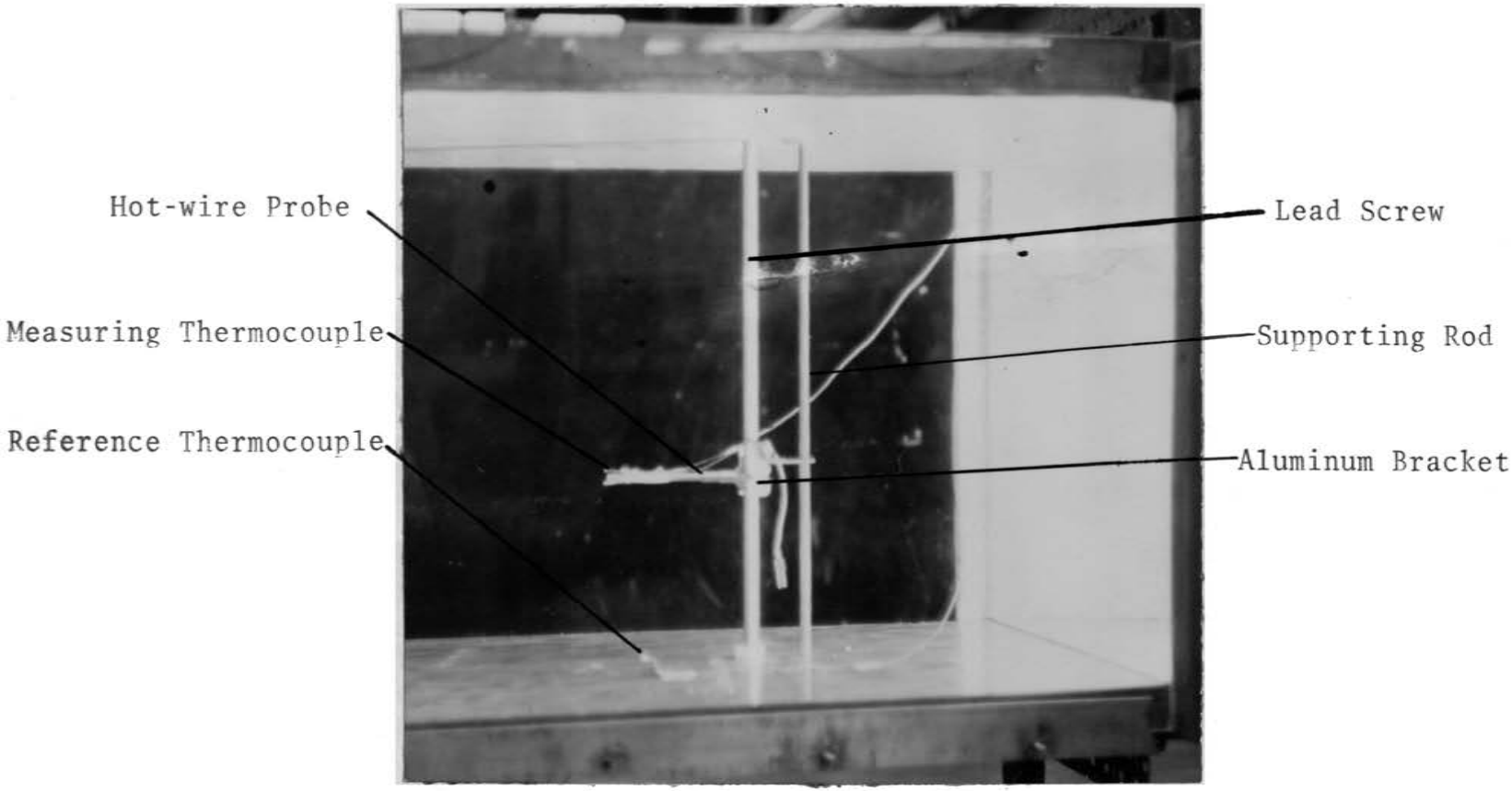


Figure 3-4. The Traversing Mechanism

# IV. RESULTS AND DISCUSSIONS

Experimental results are presented in three parts. The first deals with the velocity and temperature profiles, their validity with respect to various theories and the flow field stability represented by the Richardson number profiles. The second part presents the turbulence characteristics of the flow field and the third, a discussion of the flow field made visible by smoke tests.

## A. Velocity and Temperature Profiles

### 1. Velocity Profiles

The maximum velocity in the test section was 6.9 feet per second. The velocity and longitudinal turbulence intensity profiles at Station 2 without any profile generating apparatus in the inlet section are shown in Appendix D. These are the test section flow characteristics and they indicate a constant velocity with height except at the boundaries. The boundary layer at the floor of the test section is less than 0.5 inch thick and that at the top, about 2.0 inches. The thicker boundary layer at the top is due to the roughness of the roof of the test section caused by the many test holes drilled there. The longitudinal turbulence intensities were less than 1.0 per cent except at the boundaries where boundary layer effects caused a slightly larger value.

Measuring stations were located at distances of 1, 20 and 30 inches from the test section entrance and along the center line of the test section. Measurements were made at every one inch interval in the vertical direction at each station. The coordinate system used and the three measuring stations chosen are shown in Figure (4-1). Data were also obtained for two different conditions of flow; one in which the heating element was not operating and the other when it was. The generation of the velocity profile, as discussed in Section III, included the positioning of screen wire meshes of over-lapping thicknesses and a 2 inch high boundary layer trip made of masking tape. The boundary layer trip can also be considered as a model shelter belt, since it is primarily used to decrease the velocity of the flow at the surface. The effects of a wedge shaped shelter belt on a flow with a naturally grown boundary layer is described by PLATE, (1971) and shown in Figure (4-2). At a large distance downstream from the fence, the secondary boundary layer formed by the reattached flow generated by the wedge blends with that of the outer flow and a new and thicker boundary layer results.

The velocity profiles at station 1 are shown in Figure (4-3) where dimensionless velocities are plotted against dimensionless heights. The points plotted indicate the distorted flow caused by the screen mesh arrangement. The plot shows sharp increases in velocities where the overlap of one screen wire with the other screens end.

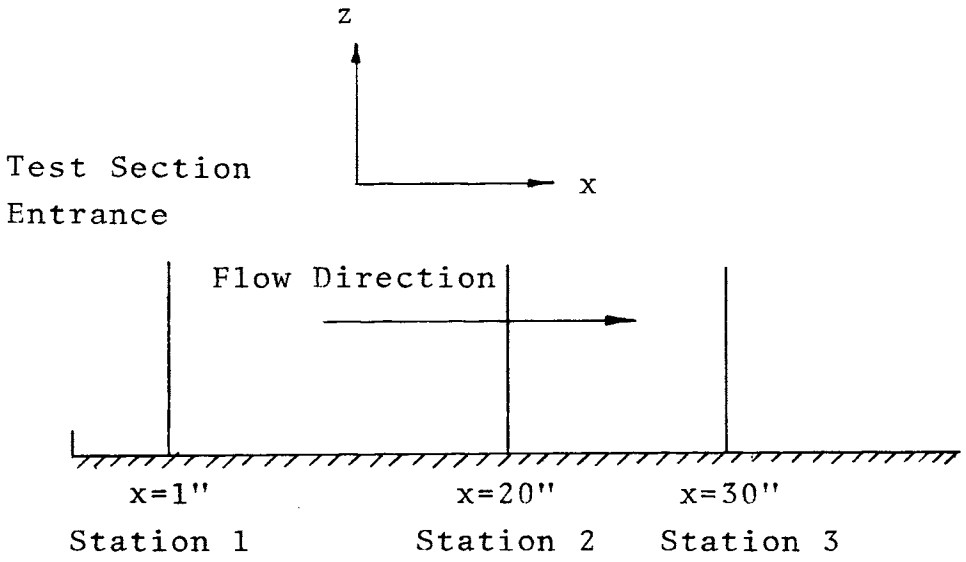


Figure 4-1. Location of Measuring Stations and Co-ordinate System

1. Standing eddy zone
2. Region of hill influence
3. Region of re-establishing secondary boundary layer
4. Blending region between middle and outer layer
5. Blending region between inner and middle layer
6. Undisturbed boundary layer
7. Potential outer flow
8. Wedge

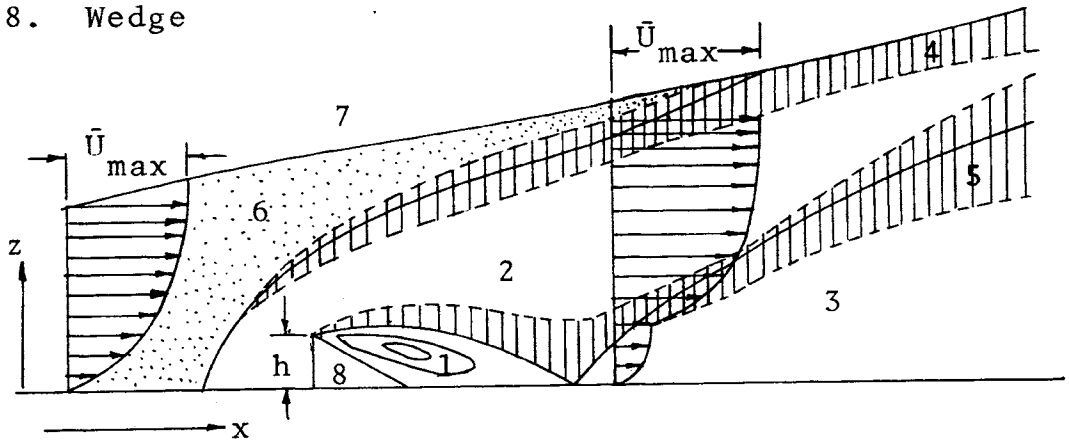


Figure 4-2. The Flow Zones of a Boundary Layer Disturbed by a Shelterbelt (PLATE & LIN, 1965)

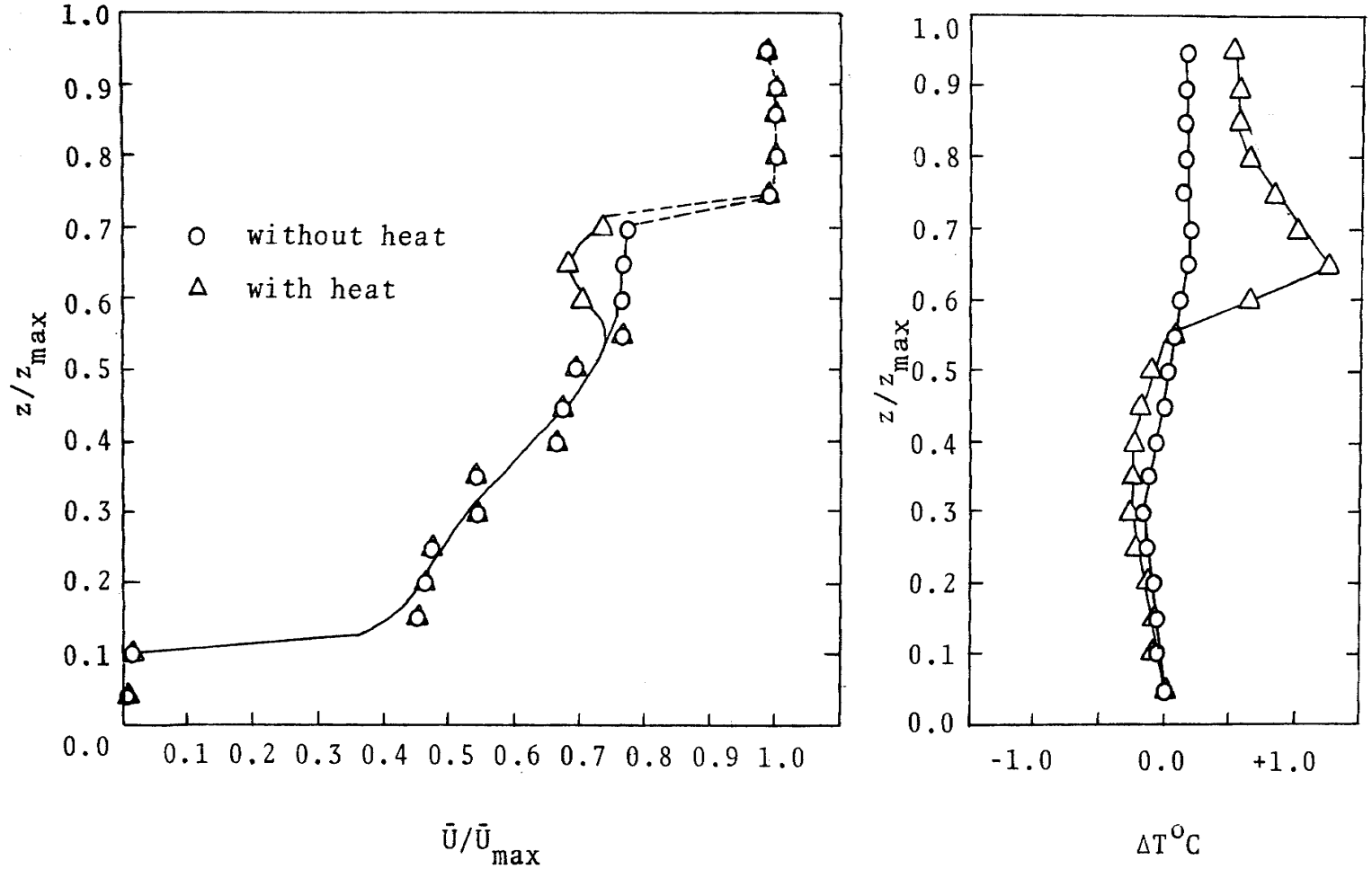


Figure 4-3. Velocity and Temperature Profiles at Station 1

This change is very marked at $z/z_{max} = 0.70$, where there is only one screen left. The velocities in the region just after the fence, ie., at $z/z_{max} = 0.05$ and 0.10, may not be that of the main flow, but of the eddy zone in region 1 of Figure (4-2). The curve for the "without heat" case shows a nearly constant velocity in the region extending from $z/z_{max} = 0.60$ to 0.70. Above $z/z_{max} = 0.70$ the velocity increases very sharply. For this reason, the height of the model boundary layer is taken as 14 inches, ie., extending from the surface to $z/z_{max} = 0.70$. The velocity profile at station 1 for the case "with heat" coincides with that of "without heat" up to $z/z_{max} = 0.55$. There is a decrease in velocity between here and $z/z_{max} = 0.70$ which results from the convective motion of the heated air mass in the inlet section.

For station 2, the velocity profiles for both the "without" and "with heat" cases are shown in Figure (4-4). The curves are smoother than at station 1. For the case "with heat" a decrease of velocity by 11 per cent as compared to the case "without heat" in the region extending from $z/z_{max} = 0.60$ to 0.70 can be seen. The secondary boundary layer caused by the trip extends to $z/z_{max} = 0.10$ from the surface. At station 3, Figure (4-5), the secondary boundary layer has grown to a height of 4 inches and has still not blended with the main boundary layer. For the type of flow shown in Figure (4-2), the secondary boundary layer blends with the outer boundary layer at some large

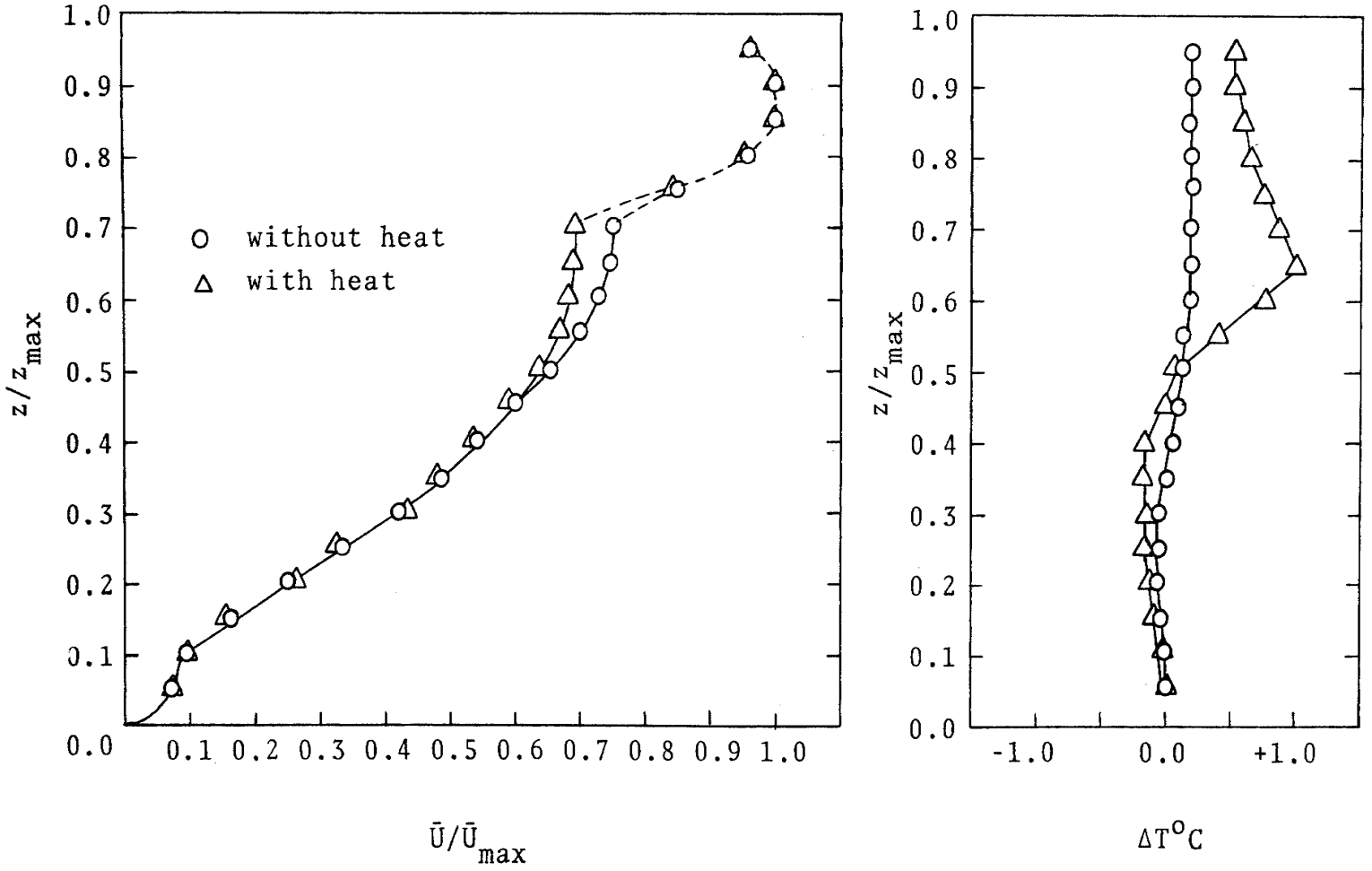


Figure 4-4. Velocity and Temperature Profiles at Station 2

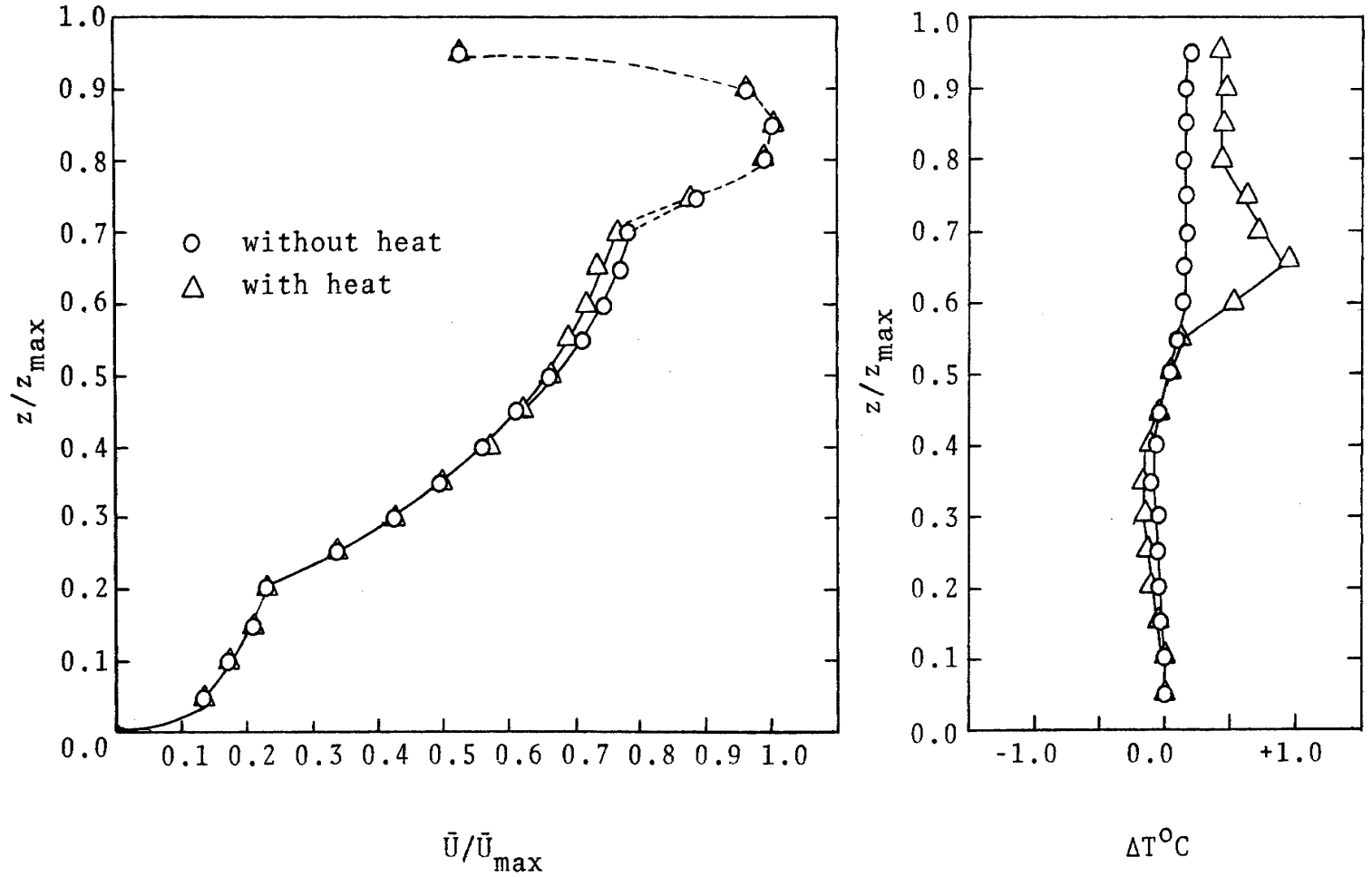


Figure 4-5. Velocity and Temperature Profiles at Station 3

distance downstream (CHANG, 1966). The type of flow in this investigation varies from that shown in Figure (4-2) in that the flow has a straight fence and not a wedge and the main boundary layer here is artificial and not natural. It can be surmised that a blending of the velocity profiles will occur at some distance further downstream. The effect of heating on the velocity profile at station 3 is minimal and results in a lower velocity at $z/z_{max} = 0.70$. The decrease in velocity was 1.5 per cent. The profiles at the last station are smoother than those at the two previous stations.

2. Temperature Profiles

Temperatures are plotted against non-dimensional heights. These temperatures are the differences between the temperature at $z/z_{max} = 0.025$ and that at the specified heights. Temperature fluctuations did exist but did not generally exceed 15 per cent. Temperatures recorded were the mean values. The temperature profiles for station 1 are shown in Figure (4-3). At this station, for the case "without heat", the temperature decreases by $0.17^{o}C$ at $z/z_{max} = 0.30$, then increases to a maximum of $0.18^{o}C$ at $z/z_{max} = 0.65$, and finally remains nearly constant. The temperature gradient between two adjacent points is assumed constant. For the case where the heat is on, the decrease in temperature in the lower half of the test section is larger. The maximum temperature of $1.25^{o}C$ occurs at $z/z_{max}$ of 0.65, while the heating element was placed at a height corresponding to $z/z_{max} = 0.50$. This upward shift of the

maximum temperature indicates convective movement of the hot air mass in the inlet section after the splitter plate. This upward movement of the air mass results in greater intake of cold air from the outside to the lower half of the test section, and accounts for the larger drop in temperature here. The temperature profiles at station 2, Figure (4-4), are similar to those at station 1. For the case "without heat" the maximum variations of temperatures are less than those at station 1. For the case "with heat" the maximum temperature increase was $1^{o}C$ and occurs at $z/z_{max} = 0.65$. This indicates that there is no large-scale convective motion in this region in the test section. At station 3, Figure (4-5), the temperature profiles are similar to those obtained at stations 1 and 2. For the case "without heat", the temperatures are less and the profile could become fully isothermal farther downstream. An isothermal temperature profile in the model would represent a neutral atmosphere, according to equation (2-42), if a reasonable scaling factor were used. For the case "with heat", the maximum temperature increase was $0.9^{o}C$ and again occurred at $z/z_{max} = 0.65$. This shows that the stable layer characterized by the maximum temperature does not move upwards. A static stability analysis, according to equation (2-13), for the temperature profile at station 3 "with heat" gives negative stability for the layer from $z/z_{max} = 0.10$ to 0.30, neutral stability for the layer from

$z/z_{max}$ = 0.30 to 0.40, a stable condition from $z/z_{max}$ = 0.40 to 0.55 and strong stability or inversion from $z/z_{max}$ = 0.55 to 0.65. From the layer $z/z_{max}$ = 0.65 to 0.80 the stability is again negative. The flow field stability does not depend on the static stability alone, but on the dynamic stability as defined by the Richardson number and the degree of stratification indicated by the turbulence characteristics of the flow field.

3. The Validity of the Temperature Profile

Using a scale factor of 240:1, the temperature profile at station 3 for the case "with heat" is scaled up to the atmosphere. Figure (4-6) shows that gradients of -18$^{o}$C per kilometer or less are obtained below the inversion. Temperature gradients of such magnitudes rarely exist in the atmosphere over long periods of time. Gradients of 56$^{o}$C per kilometer or more in the inversion layers are also obtained. It can be seen that the maximum temperature variations decrease in magnitude in the wind tunnel as the flow proceeds downstream. The profile obtained farther downstream might be a suitable representation of atmospheric temperature gradients. On the other hand, a change in scale could be made to obtain more reasonable values for atmospheric temperature gradients. This change would, however, effect other parameters of the flow, especially the velocity gradients as discussed in Section II.

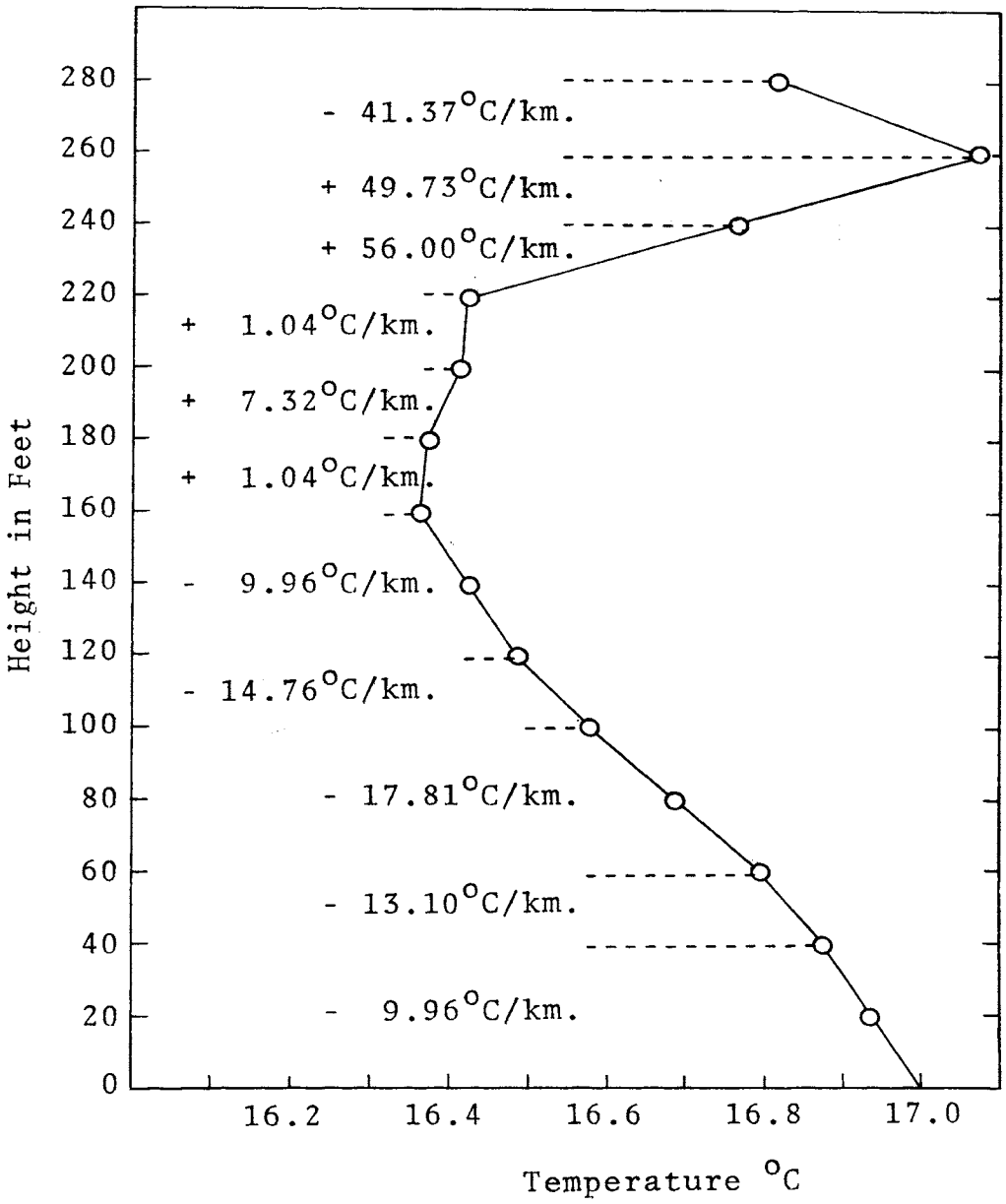


Figure 4-6. Temperature Profile Scaled from Model Profile at Station 3

4. Richardson Number Profiles

The dynamic stability as defined by the Richardson number, equation (2-30), takes into account both the temperature and velocity gradients. Richardson numbers are plotted against non-dimensional heights for stations 2 and 3, Figure (4-7). At station 2, for the "without heat" case, the Richardson numbers are confined to very small values rarely exceeding 0.04. The criteria for dynamic stability has been set at values of Richardson numbers ranging from greater than 0.25 for flows with constant velocity gradients and no density gradients, to values greater than 0.0417 for flat plate boundary layer flow with a density gradient (SCHLICHTING, 1954). A uniform parallel flow in which the velocity is constant with height is stable, although the Richardson number is everywhere zero. Local stability considerations require that the appropriate Richardson number is an "average" obtained in the vicinity of observed instabilities. A negative Richardson number indicates extreme instability. The Richardson number profile at station 2 for the case "with heat" shows values less than zero for the layer extending from $z/z_{max}$ = 0.0750 to 0.325. The values of Richardson numbers above $z/z_{max}$ = 0.425 are positive and greater than 0.24. The maximum Richardson number occurs at $z/z_{max}$ = 0.625 and has a value of 1.98. Above this point a negative value is reached. The Richardson number profiles at station 3 are similar to those at station 2, although the maximum values are less

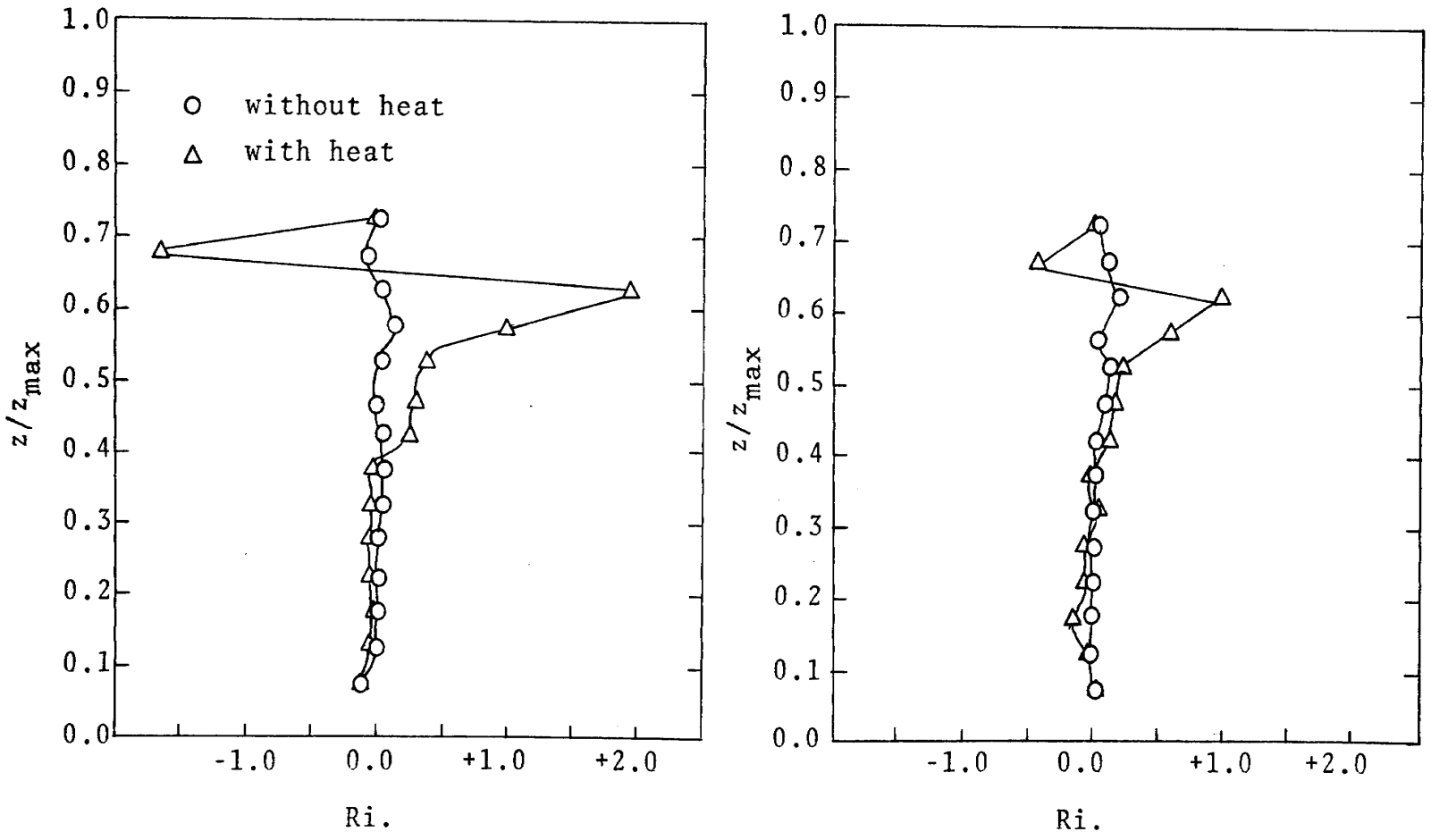


Figure 4-7. Richardson Number Profiles at Stations 2 and 3

here as the temperature and velocity gradients have decreased. The maximum Richardson number of 0.961 was at the same $z/z_{max}$.

5. The Validity of the Velocity Profiles

The velocity profile at station 3 has not developed fully. Nevertheless, an analysis is made by comparison to velocity profiles obtained from empirical and experimental data. To offset the effect of the trip on the velocity profile, a roughness length of 2 inches, equal to the height of the fence was taken into consideration for the computation of velocities from theory. Figure (4-8) shows the velocity profile at station 3, "without heat". The velocities from the log-linear law given by equation (2-17) for a fully neutral and rough flow, is shown in the same figure. The two curves show similar shapes, with a deviation occurring below $z/z_{max} = 0.2$, where the effects of the secondary boundary layer are felt.

In Figure (4-9), the velocity profile for station 3 "with heat" is shown. The log-linear law with the correction term for stability, given by equation (2-21), is shown for the values $\alpha = 3$ and 7. Corresponding values for L, the scale length, and u, the friction velocity, were taken into consideration. For the case of $\alpha = 3$, the theoretical flow is fully unstable, and the velocity profile obtained shows close resemblance to the experimental curve. Deviations occur below $z/z_{max} = 0.20$ and also in the layer $z/z_{max} = 0.50$ to 0.60 where the flow is

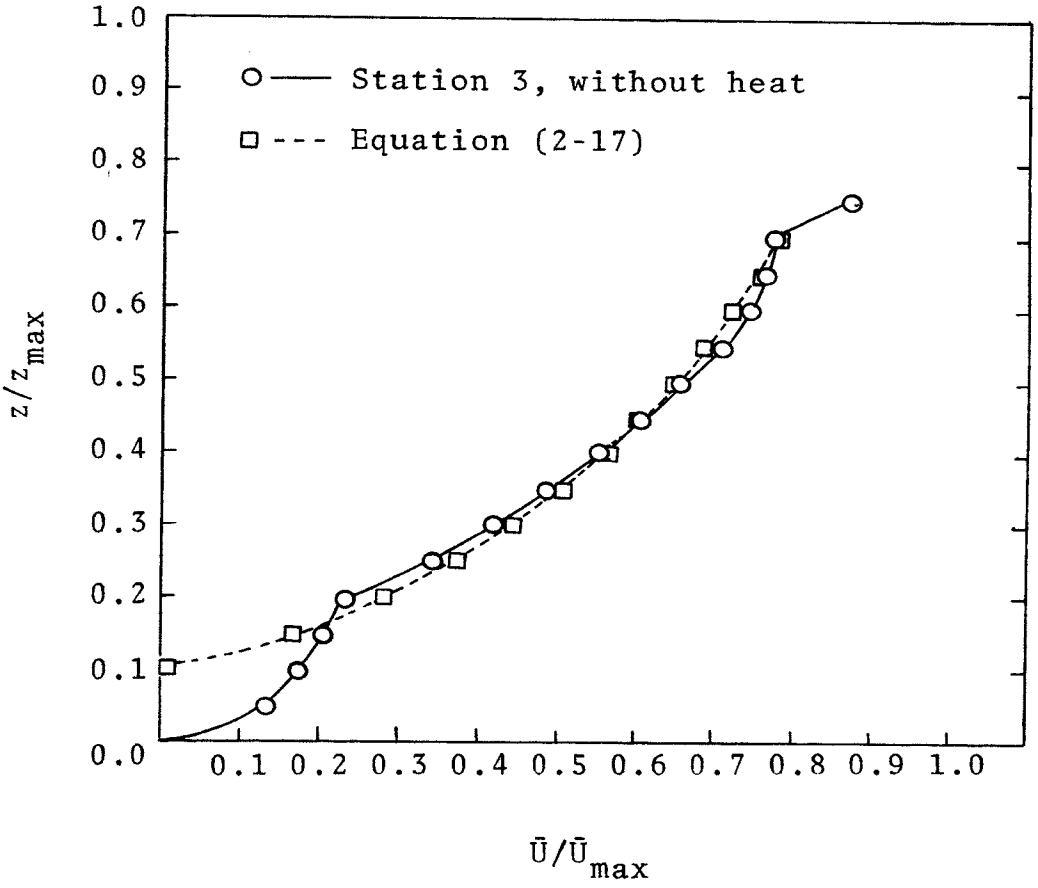


Figure 4-8. Comparison of Velocity Profile at Station 3, without heat, to Log-linear Law, Equation (2-17)

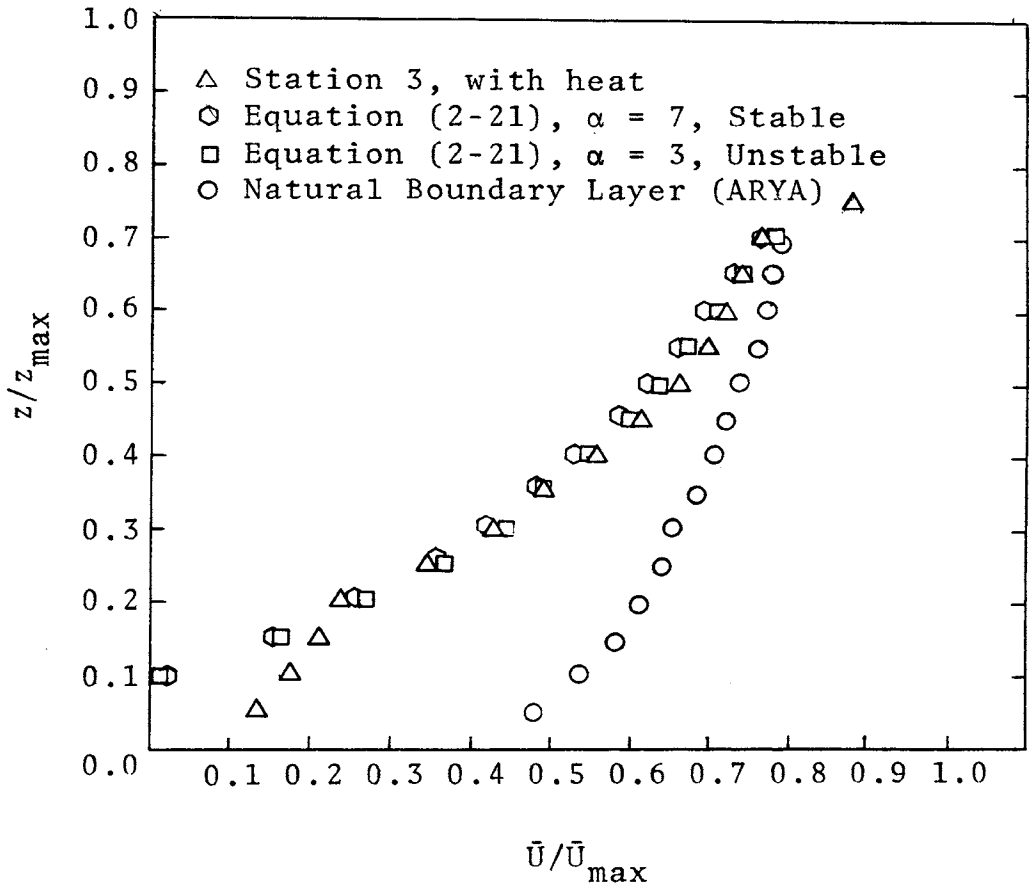


Figure 4-9. Comparison of Velocity Profile at Station 3, with heat, to Log-linear Law and Natural Boundary Layer Profile

dynamically stable. For the case $\alpha = 7$, the theoretical flow is fully stable and shows about the same relation to the experimental curve as for the case of $\alpha = 3$.

The velocity profile for a fully stable flow in a naturally grown boundary layer is also plotted in Figure (4-9). This velocity profile was obtained at a distance of 78 feet downstream of the test section in investigations on wind tunnel boundary layer flows by ARYA, (1968). The velocity profile shows that the boundary layer is fully developed and the effects of the fence are absent. The velocity profile obtained in this investigation, at station 3 as compared to that obtained by ARYA, shows that the flow has to develop further to rid itself of the effects of the fence. This can happen if either the flow is allowed to go farther downstream or by changing the height of the fence.

B. Turbulence Characteristics of the Flow

1. The Turbulence Intensities

The longitudinal and vertical turbulence intensities are plotted against dimensionless heights. Figure (4-10) shows these curves plotted for the "without heat" case at stations 2 and 3. The maximum intensity of longitudinal turbulence is 10 per cent for station 2 and occurs at $z/z_{max} = 0.20$. The maximum longitudinal turbulence intensity decreases by approximately 1 per cent by the time the flow reaches station 3. At station 3 the height of the

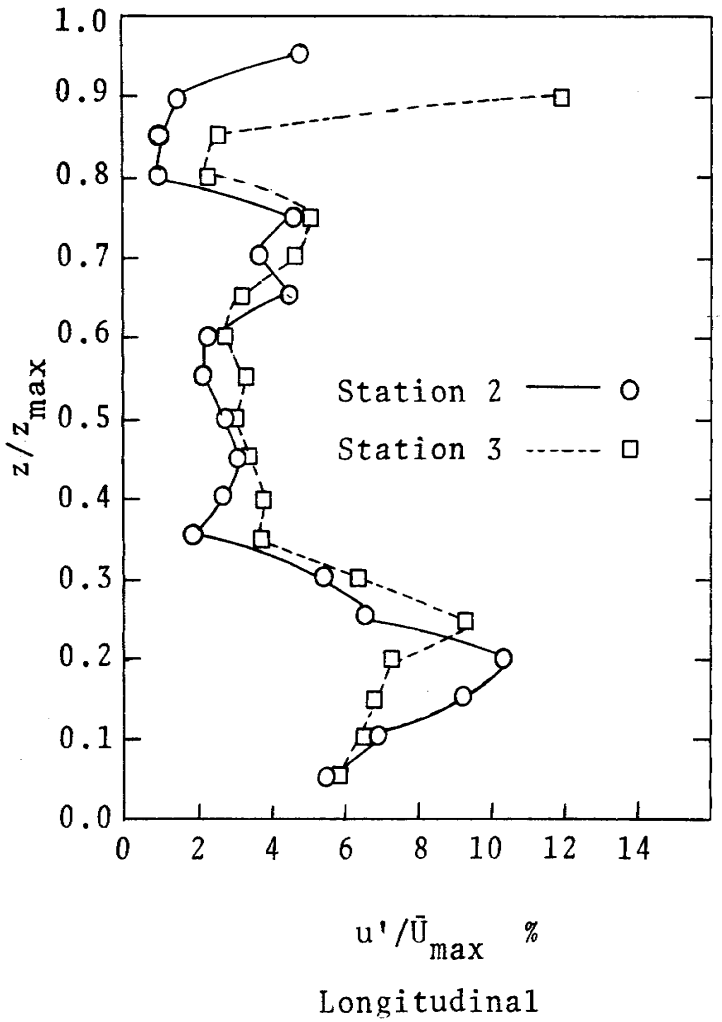


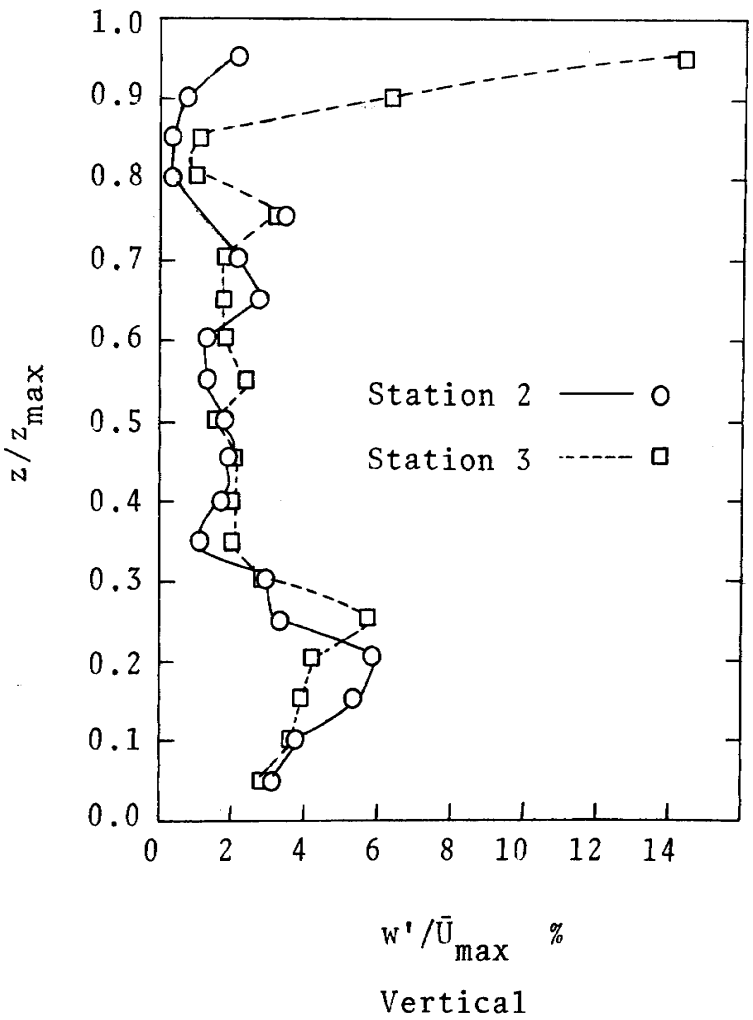


Figure 4-10. Turbulence Intensity Profiles at Stations 2 and 3, without heat

maximum longitudinal turbulence has shifted to $z/z_{max} = 0.25$. The occurrence of this high degree of turbulence in this region is due to the effects of the fence. Above the region affected by the fence, the longitudinal turbulence intensity decreases and remains between 2 and 4 per cent. There is a slight increase above $z/z_{max} = 0.70$, and this is due to the sudden increase in velocity at this height. Above $z/z_{max} = 0.85$ there is a large increase in longitudinal turbulence and this is due to the roughness of the test section roof. The curves for the longitudinal turbulence intensities between $z/z_{max} = 0.40$ and 0.70 show that the screen wire arrangement produces turbulence. The turbulence profile for station 2 is slightly more distorted than at station 3 for the region $z/z_{max} = 0.30$ to 0.60. The vertical turbulence intensities for stations 2 and 3 for the case of "without heat" are also shown in Figure (4-10). These curves are similar in shape to the longitudinal intensity profiles although their values are about half of the longitudinal intensities.

Figure (4-11) shows the same profiles for the "with heat" condition. The general shape of the turbulence intensity profiles are the same as for the "without heat" case, especially in the lower regions extending from the floor to $z/z_{max} = 0.50$. Above this height there is an increase in longitudinal turbulence intensity. This is the region of increasing temperature gradients. However, the

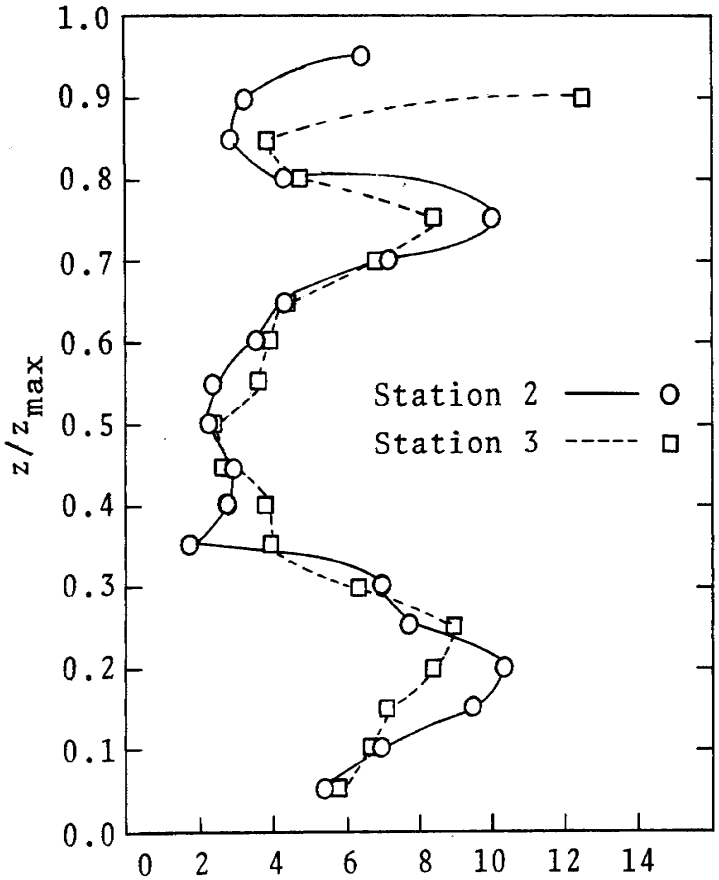


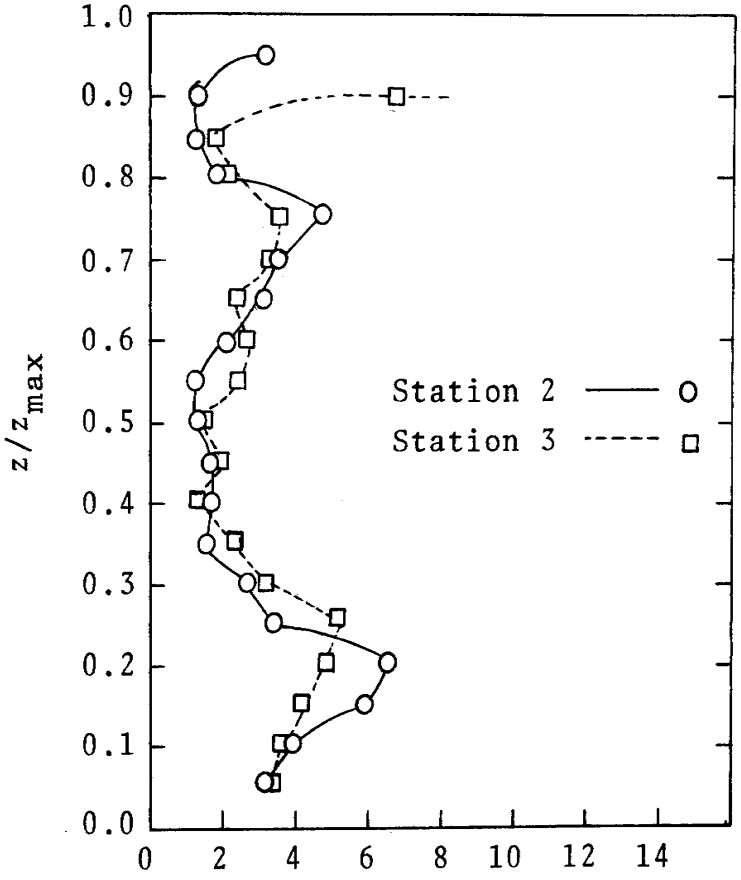


Figure 4-11. Turbulence Intensity Profiles at Stations 2 and 3, with heat

maximum temperature occurs at $z/z_{max} = 0.65$, but the maximum turbulence intensity occurs at $z/z_{max} = 0.75$. This shows that the maximum instabilities in the flow occur above the maximum temperature and not in the inversion layer.

Figure (4-12) shows the longitudinal and vertical turbulence intensities for station 3, for both cases of "without heat" and "with heat". In the region extending from the surface to $z/z_{max} = 0.55$, the effect of heating is very small. The maximum longitudinal turbulence intensity at $z/z_{max} = 0.25$ decreases by 1 per cent when the heating is on. The change due to heating, at the same point, in the vertical turbulence intensity is almost negligible. In the region of maximum temperature due to heating, the increase in longitudinal turbulence is about 1 per cent, and that for the vertical turbulence intensity slightly less. For the region above the heating, ie., above $z/z_{max} = 0.70$, the longitudinal turbulence intensity is very high and the increase is as much as 3 per cent. The increase in this same region for the vertical turbulence intensities is almost negligible.

Stable density gradients in a flow field, act so as to reduce the turbulence intensities by viscous damping. In this experiment the turbulence intensities increased, when the positive temperature gradient was introduced. This indicates that interactions exist between the turbulent motion generated primarily by the screen wire arrangement

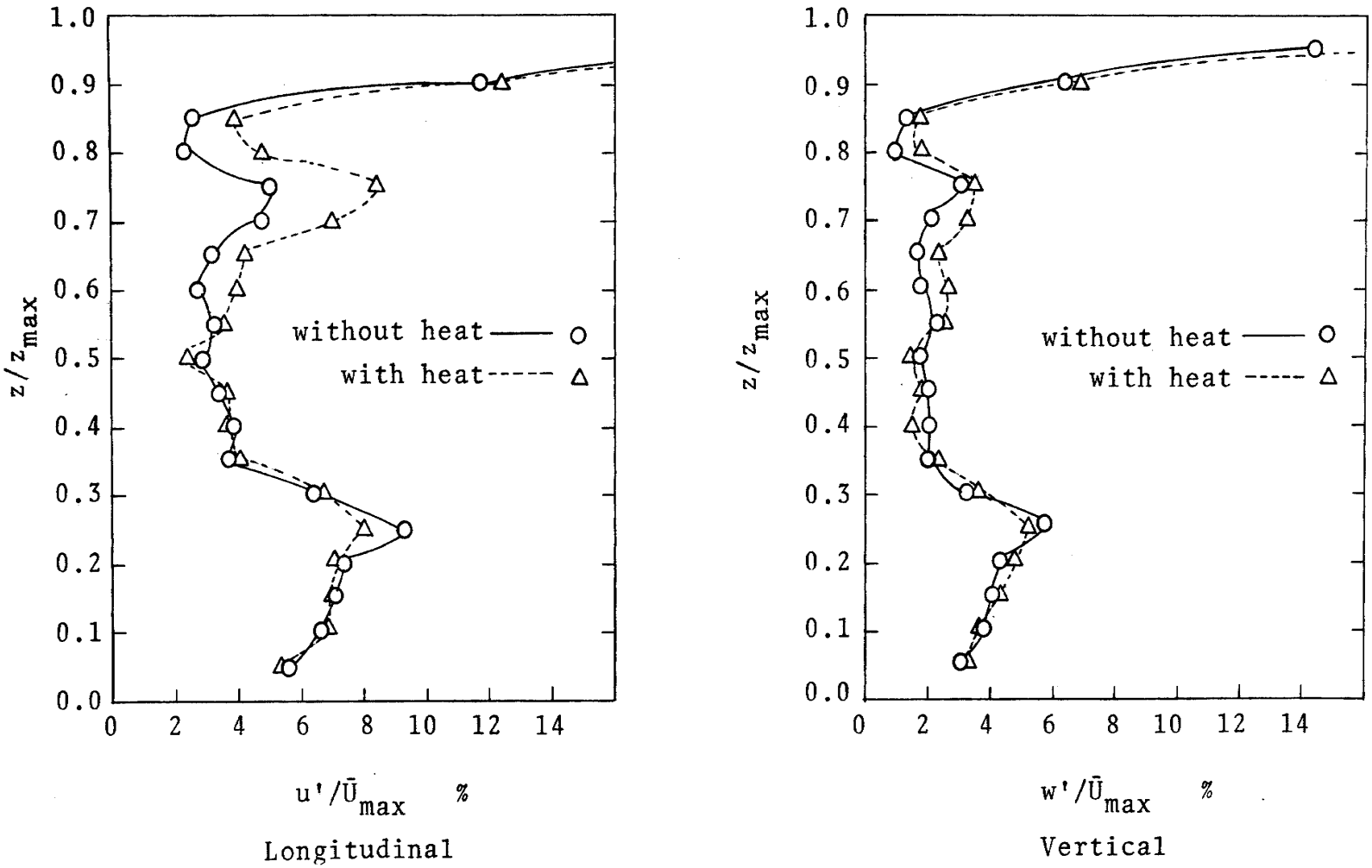


Figure 4-12. Turbulence Intensity Profiles at Station 3

and by the temperature field, generated by the heating elemet.

2. The Turbulent or Reynolds Shear Stress

The turbulent shear stresses, also called the Reynolds stresses at stations 2 and 3, are plotted in Figure (4-13) for both cases of "without heat" and "with heat". Except for two regions, one in which the effects of the fence are felt, and the other where the velocity increases sharply at $z/z_{max} = 0.70$, the shear stresses are almost constant for both stations and both heating conditions. In general, the same observations apply here as in the case of the turbulence intensity components. The constancy of shear stress with height that is essential for correct modeling has not been sufficiently achieved, especially in the lower layers. Although there is a nearly constant shear stress layer extending from $z/z_{max} = 0.30$ to 0.65, the shear stress should, in principle, decay as the flow proceeds downstream. In this case the shear stresses show increasing values downstream. This could be due to additional disturbances between stations 2 and 3.

Figure (4-14) shows the turbulent Reynolds shear stress profiles at station 3 for the cases of "without heat" and "with heat". The effect of heating on the shear stress profile is to increase the gradients in the lower layers where the influence of the fence exists and a slight

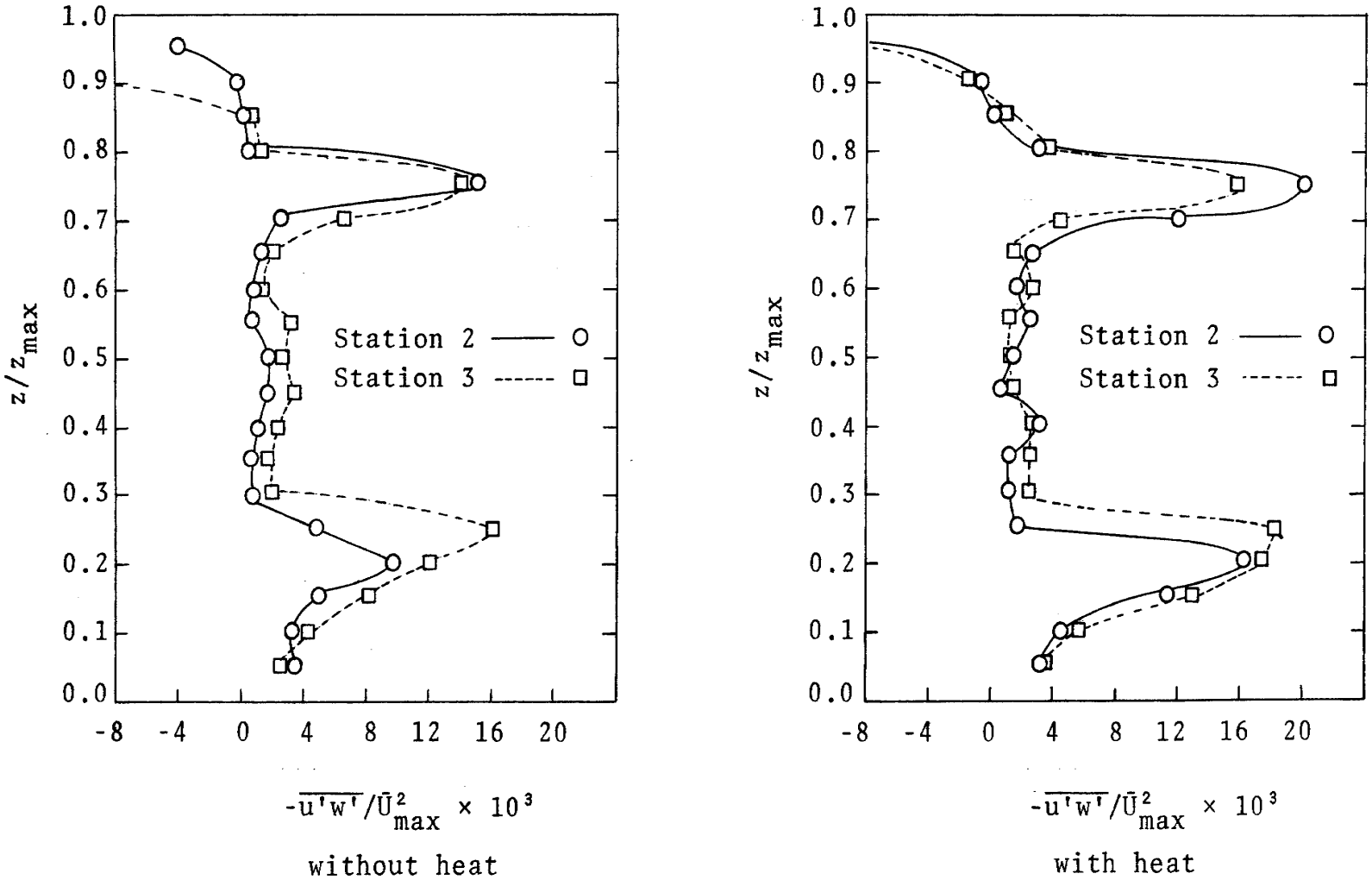


Figure 4-13. Turbulent Shear Stress Profiles at Stations 2 and 3

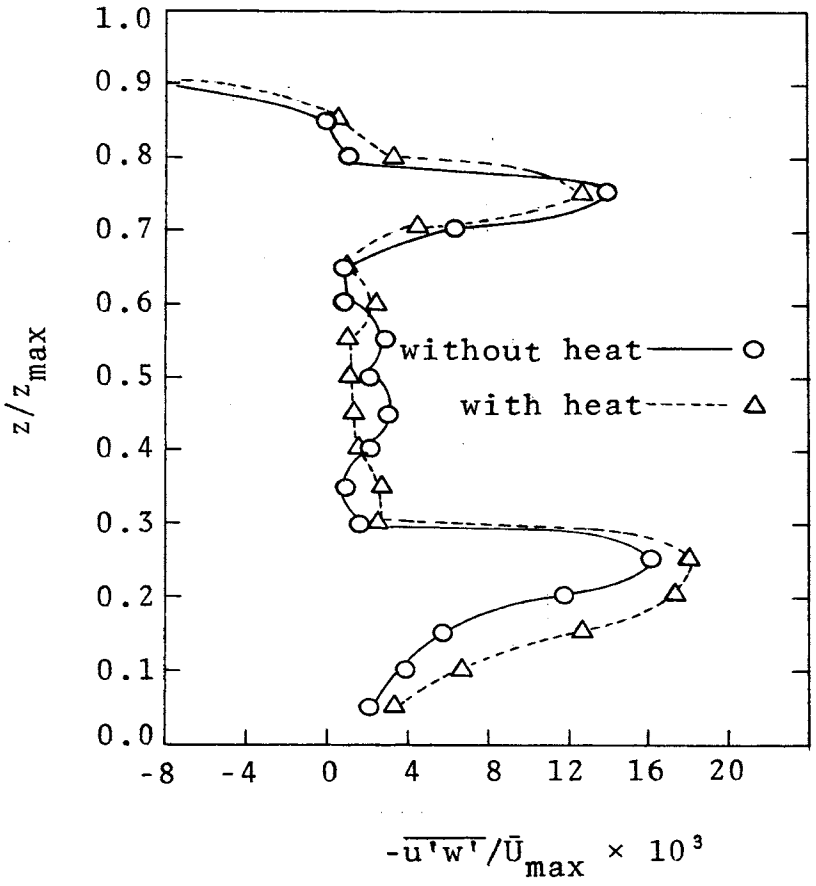


Figure 4-14. Turbulent Shear Stress Profiles at Station 3

decrease in values in the middle regions, ie., from $z/z_{max}$ = 0.35 to 0.65. To obtain constant shear stress with height in this flow, it appears necessary to match carefully the height of the fence to the roughness of the surface. In this experiment a rough floor was not used. Also, equation (2-37) requires that there should be no pressure gradients in the direction of mean flow. The maximum velocity at station 1 was 6.3 feet per second, while that at station 3 was 6.9 feet per second. This indicates that there exists a pressure gradient and that the flow is accelerating downstream.

C. Smoke Tests

A smoke generating unit was used to visualize the flow at 2.5 inch intervals and beginning at height $z/z_{max}$ = 0.05. Figure (4-15) shows the smoke streams in the flow field for the case of "without heat". The smoke stream in the layer $z/z_{max}$ = 0.05 to 0.175 show extreme turbulence as in this layer the effect of the fence is maximum. Turbulence is also noticed in the region above $z/z_{max}$ = 0.7. These observations agree quite well with the turbulence measurements. Figure (4-16) shows the smoke streams in the flow field for the case "with heat". The lower region turbulence is about the same but the smoke stream at height $z/z_{max}$ = 0.55 shows some change, though barely discernable. There appears to be a wave like configuration of this smoke stream. Further, the observation that heating does not

Figure 4-15. Smoke Streams "without heat"

Figure 4-16. Smoke Streams "with heat"

cause large scale convective motions of the heated layer is confirmed by the steady level of the smoke stream at $z/z_{max} = 0.55$ as it proceeds downstream.

A model smoke stack of 0.75 inch diameter and 9.0 inches in height, placed just 1 inch downstream of the test section entrance was used to observe the plume path in the generated model boundary layer. Figure (4-17) shows the arrangement along with the model plume. The exit velocity of the smoke from the stack could not be effectively controlled and hence the resulting plume path was not very realistic. The plume did not change its shape or path when the model inversion was generated.

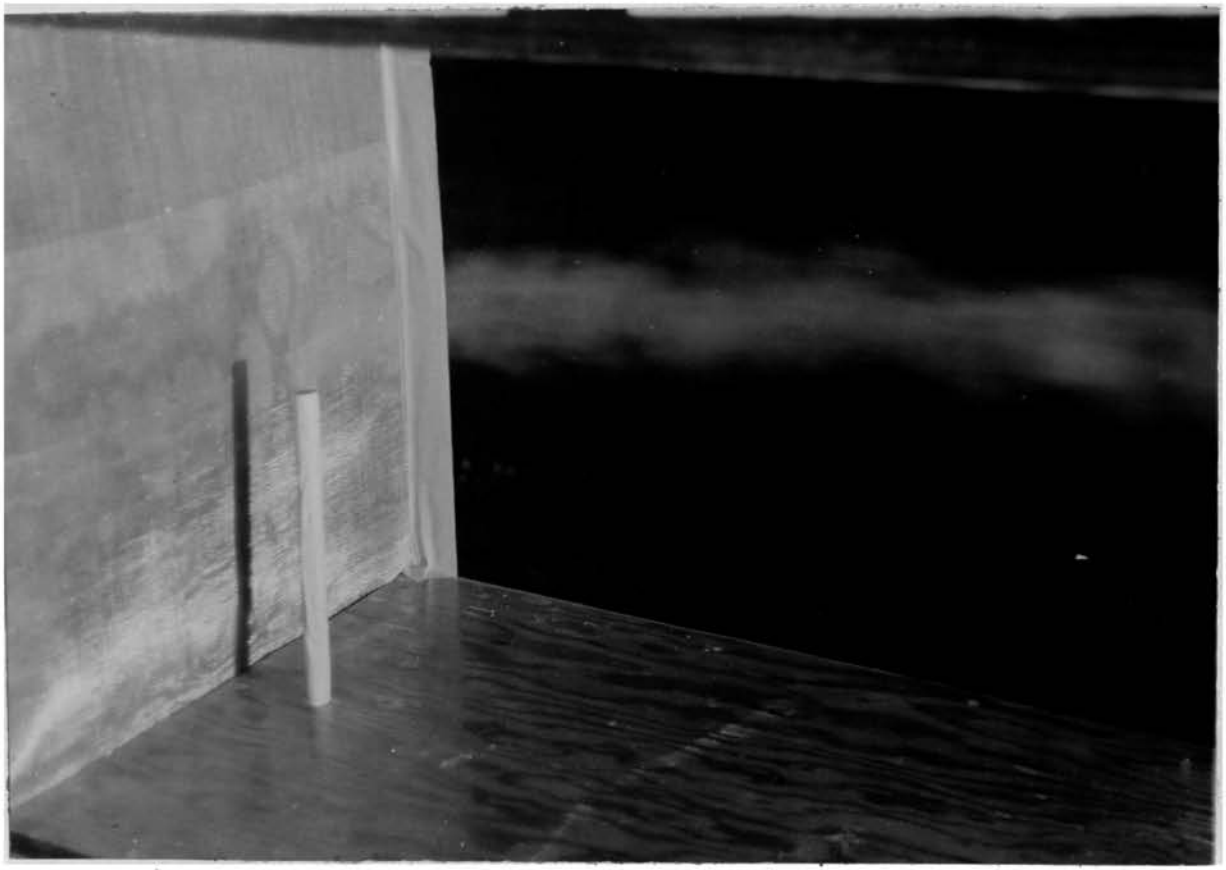

Figure 4-17. Model Smoke Stack

# V. CONCLUSIONS

The flow in the modified wind tunnel has been investigated to determine its suitability as a model for atmospheric surface boundary layers flow. The suitability of using flow profile generating apparatus are examined. It is found that the temperature profiles generated in the wind tunnel are quite representative of the atmospheric temperature profiles except near the ground. The gradients of atmospheric temperature in the layer next to the surface are relatively large due to the heat transfer processes taking place there. Such gradients of temperature at the surface of the model boundary layer were non-existent as the surface was neither heated nor cooled. The velocity profiles at the last station in the wind tunnel, though not fully developed, show similarity in shape to the theoretical log-linear law. The velocity profiles also show that a longer test section is needed if it is to develop to the shape of the velocity profile obtained by a naturally grown boundary layer. The use of roughness length in the calculations for velocity profiles show that the required velocity profiles can be attained at shorter distances downstream than would ordinarily be required by natural growth means if roughness elements were used. The turbulence characteristics of the flow field show that the flow is still in the region of the effects of the fence and a nearly constant shear stress with height could be obtained.

In summary it can be concluded that:

1. Temperature profiles representative of atmospheric conditions can be obtained by the use of apparatus at the entrance of the inlet section. However, to achieve steeper gradients at the surface, the test section floor has to be heated or cooled.

2. Velocity profiles generated by means of screen wire arrangements show promise of developing to the shape required if the test section is made longer. The use of roughness elements matching the fence height to preserve the gradients of velocity near the surface would be beneficial. The turbulence intensities in the lower regions show that the effects of the fence have not been dissipated. The flow needs further development to properly assess the suitability of the screen mesh arrangement for generating turbulence profiles.

3. Stratification in the region of the inversion layer as indicated by the turbulence characteristics of the flow is not achieved, although large convective motions are not present. The absence of equilibrium in the interaction of the temperature and velocity fields caused an increase in turbulence intensities as the flow was heated.

4. The Reynolds shear stress profiles show that a region of constant shear with height exists. With proper use of fence height and roughness elements a constant shear stress layer can be obtained. The turbulence intensity is initially too high near the ground, but the redistribution

of this turbulent energy is fairly rapid and the turbulence structure improves as the flow proceeds downstream.

5. The choice of scale length, as discussed in Section II, has to be made carefully in order to satisfy as closely as possible all the modeling parameters.

6. After initial success in modeling the basic parameters of atmospheric flow, quantities such as the integral scales of turbulence, the energy dissipation scale, the spectra of turbulence and other correlation functions should be measured.

7. Finally, the use of a small horizontal wind tunnel for these investigations was hampered by the restricted length of the test section. Nevertheless, as a pilot project the wind tunnel was suitable for reproduction of the basic parameters, namely the temperature and velocity profiles.

# VI. BIBLIOGRAPHY

Arya, S.P.S., (1968), "Structure of Stably Stratified Turbulent Boundary Layer," Ph.D. Dissertation, Colorado State University.

Batchelor, G.K., (1953), "The Conditions for Dynamic Similarity of Motion of a Frictionless Perfect Gas Atmosphere," Quarterly Journal of the Royal Meteorological Society, 79, p. 224-235, (see Lumley and Panofsky, (1964); p. 108).

Blackadar, A.K., (1960), "Structure of Turbulence and Mean Wind Profiles Within the Atmospheric Boundary Layer," Final Report, Contract No. AF 19(604)-5231, Pennsylvania State University, (see Lumley and Panofsky, (1964); p. 73).

Cermak, J.E., V.A. Sandborn, E.J. Plate, G.J. Binder, H. Chuang, R.N. Meroney and S. Ito, (1965), "Simulation of Atmospheric Motion by Wind Tunnel Flows," Technical Report, CER66JEC-VAS-EJP-GJB-HC-RNM-SI17, Colorado State University.

Chang, S.C., (1966), "Velocity Distribution in the Seperated Flow Behind a Wedge Shaped Model Hill," Unpublished M.S. Thesis, Colorado State University, (see Plate, (1971); p. 163).

Deacon, E.L., (1949), "Vertical Diffusion in the Lowest Layers of the Atmosphere," Quarterly Journal of the Royal Meteorological Society, 75, p. 89, (see Pasquill, (1962); p. 73,74).

Ellison, T.H., (1956), "Atmospheric Turbulence," Surveys in Mechanics, Edited by G.K. Batchelor and R.M. Davies, Cambridge University Press, (see Ludwig and Sundaram, (1969); p. 11).

Laikhtman, D.L., (1944), "Wind Profile and Interchange in the Surface Layers of the Atmosphere," Bulletin, Academy of Sciences U.R.S.S., 8, (see Pasquill, (1962); p. 73).

Lloyd, A., (1969), "The Generation of Shear Flow in a Wind Tunnel," Quarterly Journal of the Royal Meteorological Society, 93, p. 79-96.

Ludwig, G.R. and T.R. Sundaram, (1969), "On the Laboratory Simulation of Small Scale Atmospheric Turbulence," Technical Report CAL NO. VC-2740_S-1, AEC No. NYO-4038-1.

Lumley, J.L. and H.A. Panofsky, (1964), The Structure of Atmospheric Turbulence, John Wiley & Sons.

McVehil, G.E., (1964), "Wind and Temperature Profiles Near the Ground in Stable Stratifications," Quarterly Journal of the Royal Meteorological Society, 91, p. 136-146, (see Lumley and Panofsky, (1964); p. 118).

Monin, A.S. and A.M. Obukhov, (1954), "Fundamental Regularities of Turbulent Agitation in the Ground Layer of the Atmosphere," Tr. Geofiz. Inst., Akad. Nauk. SSSR, Sb. Statei, 24, p. 163-167, (see Plate, (1971); p. 80).

Pasquill, F., (1962), Atmospheric Diffusion, Van Nostrand.

Pepper, D.W., (1970), "Turbulent Structure in the Wake of a Sphere," M.S. Thesis, University of Missouri-Rolla, p. 70-95.

Plate, E.J., (1971), Aerodynamic Characteristics of Atmospheric Boundary Layers, AEC Critical Review Series.

Plate, E.J. and C.Y. Lin, (1965), "The Velocity Field Downstream from a Two Dimensional Model Hill," Final Report, Part I, to U.S. Army Material Agency, (see Plate, (1971); p. 160).

Schlichting, H., (1968), Boundary Layer Theory, 6th. Edition McGraw-Hill.

Strom, G.H., (1966), "Simulation of Atmospheric Processes in a Wind Tunnel," On Atmospheric Simulation: A Colloquium, Edited by G.M. Hidy, NCAR. Technical Note, TN-22.

Sutton, O.G., (1953), Micrometeorology, McGraw-Hill.

Wanta, R.C., (1968), "Meteorology and Air Pollution," Air Pollution, Edited by A.C. Stern, Second Edition, Volume I, Academic Press.

Webb, E.K., (1970), "Profile Relationships: The Log-linear Range, and Extension to Strong Stability," Quarterly Journal of the Royal Meteorological Society, 96, p. 67-80.

# VITA

The author, Sreemanth Pagadala, was born on December 21, 1946, in Madras, India. He graduated from the College of Engineering, Osmania University, Hyderabad, India in June 1968, and received the degree of Bachelor of Engineering in Mechanical Engineering. He enrolled in the Graduate School of the University of Missouri-Rolla in January 1969.

The author joined the Graduate Center for Cloud Physics Research in November, 1969, and has worked as a research assistant until the present time under Themis Contract N00014-68-A-0497.

# APPENDICES

# APPENDIX A

## Velocity, Temperature and Turbulence Data

## &

## Richardson Numbers

Velocity and Temperature Data at Station 1

| # | $z/z_{max}$ | $\bar{U}/\bar{U}_{max}$ (without heat) | $\bar{U}/\bar{U}_{max}$ (with heat) | $\Delta T^{o}C$ (without heat) | $\Delta T^{o}C$ (with heat) |
|---|---|---|---|---|---|
| 1 | 0.05 | 0.0025 | 0.0025 | 0.00 | 0.00 |
| 2 | 0.10 | 0.0228 | 0.0228 | -0.02 | -0.05 |
| 3 | 0.15 | 0.4519 | 0.4519 | -0.05 | -0.05 |
| 4 | 0.20 | 0.4635 | 0.4635 | -0.12 | -0.10 |
| 5 | 0.25 | 0.4748 | 0.4748 | -0.15 | -0.20 |
| 6 | 0.30 | 0.5468 | 0.5468 | -0.17 | -0.25 |
| 7 | 0.35 | 0.5468 | 0.5468 | -0.12 | -0.25 |
| 8 | 0.40 | 0.6643 | 0.6643 | -0.07 | -0.25 |
| 9 | 0.45 | 0.6782 | 0.6782 | 0.00 | -0.20 |
| 10 | 0.50 | 0.6920 | 0.6920 | 0.02 | -0.12 |
| 11 | 0.55 | 0.7638 | 0.7638 | 0.05 | 0.00 |
| 12 | 0.60 | 0.7638 | 0.7062 | 0.12 | 0.65 |
| 13 | 0.65 | 0.7638 | 0.6835 | 0.18 | 1.25 |
| 14 | 0.70 | 0.7785 | 0.7347 | 0.12 | 1.00 |
| 15 | 0.75 | 0.9975 | 0.9975 | 0.12 | 0.85 |
| 16 | 0.80 | 1.0000 | 1.0000 | 0.15 | 0.66 |
| 17 | 0.85 | 1.0000 | 1.0000 | 0.14 | 0.55 |
| 18 | 0.90 | 1.0000 | 1.0000 | 0.15 | 0.55 |
| 19 | 0.95 | 0.9833 | 0.9833 | 0.17 | 0.52 |

$\bar{U}_{max}$ = 6.314 fps  $T_{ref}$ = 27.2°C

Velocity and Temperature Data at Station 2

| # | $z/z_{max}$ | $\bar{U}/\bar{U}_{max}$ (without heat) | $\bar{U}/\bar{U}_{max}$ (with heat) | $\Delta T^{o}C$ (without heat) | $\Delta T^{o}C$ (with heat) |
|---|---|---|---|---|---|
| 1 | 0.05 | 0.0722 | 0.0781 | 0.00 | 0.00 |
| 2 | 0.10 | 0.0915 | 0.0942 | -0.05 | -0.02 |
| 3 | 0.15 | 0.1613 | 0.1623 | -0.05 | -0.05 |
| 4 | 0.20 | 0.2500 | 0.2630 | -0.07 | -0.07 |
| 5 | 0.25 | 0.3324 | 0.3213 | -0.05 | -0.12 |
| 6 | 0.30 | 0.4225 | 0.4225 | -0.05 | -0.15 |
| 7 | 0.35 | 0.4825 | 0.4823 | 0.00 | -0.17 |
| 8 | 0.40 | 0.4854 | 0.4821 | 0.05 | -0.17 |
| 9 | 0.45 | 0.6003 | 0.6003 | 0.10 | 0.05 |
| 10 | 0.50 | 0.6520 | 0.6430 | 0.10 | 0.05 |
| 11 | 0.55 | 0.7020 | 0.6754 | 0.12 | 0.40 |
| 12 | 0.60 | 0.7372 | 0.6833 | 0.17 | 0.75 |
| 13 | 0.65 | 0.7480 | 0.6852 | 0.17 | 1.00 |
| 14 | 0.70 | 0.7500 | 0.6902 | 0.16 | 0.85 |
| 15 | 0.75 | 0.8532 | 0.8486 | 0.17 | 0.57 |
| 16 | 0.80 | 0.9670 | 0.9517 | 0.16 | 0.65 |
| 17 | 0.85 | 1.0000 | 1.0000 | 0.17 | 0.57 |
| 18 | 0.90 | 1.0000 | 1.0000 | 0.17 | 0.53 |
| 19 | 0.95 | 0.9670 | 0.9670 | 0.17 | 0.52 |

$\bar{U}_{max}$ = 6.528 fps $T_{ref}$ = 27.1$^{o}$C

Velocity and Temperature Data at Station 3

| # | $z/z_{max}$ | $\bar{U}/\bar{U}_{max}$ (without heat) | $\bar{U}/\bar{U}_{max}$ (with heat) | $\Delta T^{o}C$ (without heat) | $\Delta T^{o}C$ (with heat) |
|---|---|---|---|---|---|
| 1 | 0.05 | 0.1331 | 0.1331 | 0.00 | 0.00 |
| 2 | 0.10 | 0.1722 | 0.1722 | 0.00 | 0.00 |
| 3 | 0.15 | 0.2053 | 0.2053 | -0.02 | -0.02 |
| 4 | 0.20 | 0.2364 | 0.2323 | -0.04 | -0.07 |
| 5 | 0.25 | 0.3419 | 0.3400 | -0.06 | -0.12 |
| 6 | 0.30 | 0.4208 | 0.4208 | -0.07 | -0.15 |
| 7 | 0.35 | 0.4900 | 0.4900 | -0.10 | -0.15 |
| 8 | 0.40 | 0.5534 | 0.5597 | -0.07 | -0.15 |
| 9 | 0.45 | 0.6089 | 0.6110 | -0.05 | -0.08 |
| 10 | 0.50 | 0.6578 | 0.6588 | 0.02 | 0.03 |
| 11 | 0.55 | 0.7100 | 0.6913 | 0.13 | 0.10 |
| 12 | 0.60 | 0.7496 | 0.7199 | 0.14 | 0.52 |
| 13 | 0.65 | 0.7620 | 0.7380 | 0.15 | 0.90 |
| 14 | 0.70 | 0.7780 | 0.7611 | 0.16 | 0.70 |
| 15 | 0.75 | 0.8710 | 0.8710 | 0.15 | 0.62 |
| 16 | 0.80 | 0.9840 | 0.9840 | 0.13 | 0.42 |
| 17 | 0.85 | 1.0000 | 1.0000 | 0.15 | 0.45 |
| 18 | 0.90 | 0.9580 | 0.9520 | 0.16 | 0.45 |
| 19 | 0.95 | 0.5268 | 0.5269 | 0.17 | 0.42 |

$\bar{U}_{max}$ = 6.856 fps  $T_{ref}$ = 27.1$^{o}$C

Turbulence Data at Station 2

| # | $z/z_{max}$ | $u'/\bar{U}_{max}$% without heat | $u'/\bar{U}_{max}$% with heat | $w'/\bar{U}_{max}$% without heat | $w'/\bar{U}_{max}$% with heat | $-\overline{u'w'}/\bar{U}^2_{max}$ without heat | $-\overline{u'w'}/\bar{U}^2_{max}$ with heat |
|---|---|---|---|---|---|---|---|
| 1 | 0.05 | 5.450 | 5.350 | 3.065 | 3.120 | 0.00310 | 0.00340 |
| 2 | 0.10 | 6.840 | 6.860 | 3.710 | 3.921 | 0.00300 | 0.00420 |
| 3 | 0.15 | 9.200 | 9.482 | 5.211 | 5.931 | 0.00920 | 0.01160 |
| 4 | 0.20 | 10.334 | 10.231 | 5.854 | 6.463 | 0.00949 | 0.01620 |
| 5 | 0.25 | 6.586 | 6.778 | 3.309 | 3.402 | 0.00440 | 0.00180 |
| 6 | 0.30 | 5.400 | 5.889 | 2.933 | 2.740 | 0.00058 | 0.00110 |
| 7 | 0.35 | 1.812 | 1.590 | 1.078 | 1.522 | 0.00052 | 0.00110 |
| 8 | 0.40 | 2.772 | 2.768 | 1.719 | 1.632 | 0.00071 | 0.00320 |
| 9 | 0.45 | 3.000 | 3.000 | 1.863 | 1.610 | 0.00159 | 0.00052 |
| 10 | 0.50 | 2.738 | 2.170 | 1.700 | 1.278 | 0.00140 | 0.00130 |
| 11 | 0.55 | 2.150 | 2.157 | 1.271 | 1.232 | 0.00064 | 0.00241 |
| 12 | 0.60 | 2.223 | 3.432 | 1.243 | 2.053 | 0.00063 | 0.00181 |
| 13 | 0.65 | 4.511 | 4.484 | 2.750 | 3.077 | 0.00084 | 0.00240 |
| 14 | 0.70 | 3.370 | 7.382 | 2.132 | 3.580 | 0.00231 | 0.01221 |
| 15 | 0.75 | 4.600 | 9.919 | 3.411 | 4.642 | 0.01541 | 0.02054 |
| 16 | 0.80 | 0.879 | 4.230 | 0.263 | 1.955 | 0.00015 | 0.00321 |
| 17 | 0.85 | 0.992 | 2.842 | 0.360 | 1.265 | 0.00007 | 0.00006 |
| 18 | 0.90 | 1.524 | 3.110 | 0.689 | 1.357 | -0.00024 | -0.00071 |
| 19 | 0.95 | 4.800 | 6.589 | 2.033 | 3.076 | -0.00410 | -0.00511 |

Turbulence Data at Station 3

| # | $z/z_{max}$ | $u'/\bar{U}_{max}$% without heat | $u'/\bar{U}_{max}$% with heat | $w'/\bar{U}_{max}$% without heat | $w'/\bar{U}_{max}$% with heat | $-\overline{u'w'}/\bar{U}^2_{max}$ without heat | $-\overline{u'w'}/\bar{U}^2_{max}$ with heat |
|---|---|---|---|---|---|---|---|
| 1 | 0.05 | 5.721 | 5.746 | 2.983 | 3.220 | 0.00231 | 0.00350 |
| 2 | 0.10 | 6.492 | 6.640 | 3.767 | 3.702 | 0.00411 | 0.00674 |
| 3 | 0.15 | 6.870 | 7.020 | 3.977 | 4.028 | 0.00600 | 0.01282 |
| 4 | 0.20 | 7.210 | 8.388 | 4.162 | 4.820 | 0.01205 | 0.01748 |
| 5 | 0.25 | 9.209 | 8.761 | 5.711 | 5.062 | 0.01633 | 0.01810 |
| 6 | 0.30 | 6.384 | 6.233 | 3.117 | 3.070 | 0.00189 | 0.00254 |
| 7 | 0.35 | 3.632 | 3.939 | 1.939 | 2.230 | 0.00130 | 0.00271 |
| 8 | 0.40 | 3.806 | 3.887 | 1.980 | 1.400 | 0.00233 | 0.00233 |
| 9 | 0.45 | 3.311 | 2.749 | 1.918 | 1.720 | 0.00330 | 0.00152 |
| 10 | 0.50 | 2.980 | 2.390 | 1.763 | 1.401 | 0.00221 | 0.00110 |
| 11 | 0.55 | 3.234 | 3.522 | 2.243 | 2.425 | 0.00312 | 0.00120 |
| 12 | 0.60 | 2.748 | 3.892 | 1.782 | 2.600 | 0.00100 | 0.00250 |
| 13 | 0.65 | 3.086 | 4.129 | 1.673 | 2.230 | 0.00110 | 0.00151 |
| 14 | 0.70 | 4.674 | 6.944 | 2.100 | 3.146 | 0.00650 | 0.00440 |
| 15 | 0.75 | 5.000 | 8.323 | 3.010 | 3.460 | 0.01420 | 0.01270 |
| 16 | 0.80 | 2.278 | 4.744 | 0.950 | 1.865 | 0.00133 | 0.00344 |
| 17 | 0.85 | 2.428 | 3.900 | 1.221 | 1.730 | 0.00050 | 0.00005 |
| 18 | 0.90 | 11.850 | 12.408 | 6.264 | 6.679 | -0.01000 | -0.00860 |
| 19 | 0.95 | 23.890 | 26.410 | 14.333 | 16.483 | -0.09280 | -0.29050 |

Richardson Numbers at Stations 2 and 3

| # | $z_2$ | $z_1$ | $z/z_{max}$ | Station 2 Ri (without heat) | Station 2 Ri (with heat) | Station 3 Ri (without heat) | Station 3 Ri (with heat) |
|---|---|---|---|---|---|---|---|
| 1 | 2 | 1 | 0.075 | -0.1295 | -0.1942 | 0.0004 | 0.0004 |
| 2 | 3 | 2 | 0.125 | 0.0001 | -0.0172 | -0.0517 | -0.0412 |
| 3 | 4 | 3 | 0.175 | -0.0063 | -0.0172 | -0.0349 | -0.1553 |
| 4 | 5 | 4 | 0.225 | 0.0076 | -0.0372 | -0.0040 | -0.0097 |
| 5 | 6 | 5 | 0.275 | 0.0000 | -0.0312 | -0.00364 | -0.0105 |
| 6 | 7 | 6 | 0.325 | 0.0299 | -0.0192 | -0.0138 | 0.0001 |
| 7 | 8 | 7 | 0.375 | 0.0364 | 0.0003 | 0.0191 | 0.0001 |
| 8 | 9 | 8 | 0.425 | 0.0403 | 0.2407 | 0.0132 | 0.0639 |
| 9 | 10 | 9 | 0.475 | 0.0002 | 0.3001 | 0.0615 | 0.1045 |
| 10 | 11 | 10 | 0.525 | 0.0221 | 0.3674 | 0.1004 | 0.1664 |
| 11 | 12 | 11 | 0.575 | 0.1406 | 0.9802 | 0.0146 | 0.5980 |
| 12 | 13 | 12 | 0.625 | 0.0019 | 1.9454 | 0.1621 | 0.9619 |
| 13 | 14 | 13 | 0.675 | -0.0849 | -1.6762 | 0.0912 | -0.4539 |
| 14 | 15 | 14 | 0.725 | 0.0026 | -0.0062 | -0.0026 | -0.0150 |

# APPENDIX B

## Temperature Scaling

Temperature gradients in the model can be scaled up to atmospheric gradients by using equation (2-44). Scaling is illustrated by the following example.

Equation (2-44) is

$$\frac{\delta}{T}\left[\frac{dT}{dz} + \Gamma\right]_{model} = \frac{\delta}{T}\left[\frac{dT}{dz} + \Gamma\right]_{atm.}$$

For the layer in the model extending from 12 inches to 13 inches the gradient of temperature is $+0.38^{o}C$ per inch. The following values are assigned to the various parameters

$T_{model} = 300.10^{o}K.$

$T_{atm.} = 287.00^{o}K.$

$\frac{dT}{dz}_{model} = +0.38^{o}C$ per inch

$\Gamma$ = Adiabatic lapse rate = $0.0002505^{o}C$ per inch

$\delta_{model} : \delta_{atm.} :: 1 : 240$

Substituting these values into the above equation the atmospheric temperature gradient is

$$\frac{dT}{dz}_{atm.} = \frac{287.0}{300.1} \times \frac{1}{240} \times (0.38 + 0.0002505) - 0.0002505$$

which when calculated comes out to +49.73°C per kilometer. The heights 12 and 13 inches are multiplied by the scale factor 240, to give the actual heights in the atmosphere where this temperature gradient occur. The layer then has heights between

$$\frac{12 \times 240}{12} = 240 \text{ feet}$$

and

$$\frac{13 \times 240}{12} = 260 \text{ feet.}$$

# APPENDIX C

## Data Reduction Technique

## &

## Richardson Numbers Computation

PROGRAM FOR COMPUTATION OF VELOCITIES AND LONGITUDINAL TURBULENCE : WANG CALCULATOR

( STRAIGHT WIRE ANEMOMETRY )

The bridge voltages at both zero flow and flow conditions, and the root-mean-square values of the bridge voltages at various velocities are fed into the Wang Computer. The program is written as follows:

```
07 - Mark
60 - 0
01 - Stop
     Enter the value of V
06 - Continue
24 - Write
23 - Special Format
13 - Store Full (in)
61 - 1
50 - Clear Adder (Right)
63 - 3
75 - .    (Reference Voltage)
63 - 3
70 - 8
52 - Add
62 - 2
75 - .    (Bridge Voltage at zero flow)
70 - 8
53 - Subtract
45 - Square
13 - Store Full (in)
62 - 2
56 - Clear Adder (Left)
17 - Recall Full (from)
61 - 1
56 - Add
62 - 2
75 - .
70 - 8
57 - Subtract
45 - Square
41 - Enter
17 - Recall Full (from)
62 - 2
47 - Divide
41 - Enter
```

```
66 - 6
75 - .  (Reference Velocity)
60 - 0
46 - Multiply
24 - Write
23 - Special Format
13 - Store Full (in)
63 - 3
76 - Clear Display
62 - 2
75 - .
70 - 8
41 - Enter
17 - Recall Full (from)
61 - 1
47 - Divide
45 - Square
50 - Clear Adder (Right)
53 - Subtract
61 - 1
75 - .
60 - 0
52 - Add
41 - Enter
17 - Recall Full (from)
61 - 1
46 - Multiply
13 - Store Full (in)
64 - 4
01 - Stop
     Enter the value of r.m.s. Bridge
     Voltage
06 - Continue
41 - Enter
64 - 4
75 - .
60 - 0
46 - Multiply
41 - Enter
17 - Recall Full (in)
64 - 4
47 - Divide
41 - Enter
17 - Recall Full
63 - 3
46 - Multiply
24 - Write
23 - Special Format
24 - Write
71 - 9          (Carriage Return)
02 - Search
60 - 0
```

To run the program, first, enter the value of the bridge voltage and press the Continue key. After the velocity is printed out then enter the r.m.s. bridge voltage and again press the Continue key.

This program will compute and print the values of 1. $\bar{U}$ (velocity) and 2. $u'/\bar{U}$ (longitudinal turbulence intensity)

PROGRAM TO COMPUTE LONGITUDINAL AND VERTICAL TURBULENCE INTENSITIES AS WELL AS REYNOLDS SHEAR STRESS ( X-WIRE ANEMOMETRY)

The bridge voltages at both zero flow and flow conditions, and the root-mean-square values from the sum and difference correlator at various velocities are fed into the Wang Computer. The program is as follows:

```
07 - Mark
60 - 0
01 - Stop
     Enter the value of bridge voltage
06 - Continue
24 - Write
22 - Special Format
13 - Store Full (in)
61 - 1
62 - 2
75 - .      (Voltage at zero velocity)
67 - 7
62 - 2
41 - Enter
17 - Recall Full (from)
61 - 1
47 - Divide
45 - Square
50 - Clear Adder (Right)
53 - Subtract
61 - 1
75 - .
60 - 0
52 - Add
13 - Store Full (in)
62 - 2
61 - 1
75 - .
64 - 4
61 - 1
64 - 4
41 - Enter
17 - Recall Full (from)
62 - 2
47 - Divide
41 - Enter
```

17 - Recall Full (from)
61 - 1
47 - Divide
13 - Store Full (in)
63 - 3
01 - Stop
Enter the value of $e_{sum}$ (r.m.s.)
06 - Continue
41 - Enter
17 - Recall Full (from)
63 - 3
46 - Multiply
24 - Write
22 - Special Format
01 - Stop
Enter the value of $e_{diff}$ (r.m.s.)
06 - Continue
41 - Enter
17 - Recall Full (from)
63 - 3
46 - Multiply
24 - Write
22 - Special Format
01 - Stop
Enter the value of $R_{AB}$ (Correlater)
06 - Continue
13 - Store Full (in)
64 - 4
17 - Recall Full (from)
62 - 2
41 - Enter
17 - Recall Full (from)
61 - 1
46 - Multiply
45 - Square
13 - Store Full (in)
65 - 5
17 - Recall Full (from)
64 - 4
41 - Enter
64 - 4
75 - .
60 - 0
46 - Multiply
41 - Enter
17 - Recall Full (from)
65 - 5
47 - Divide
24 - Write
23 - Special Format
24 - Write (Carriage Return)
71 - 9

02 - Search
60 - 0

The procedure for running this program is as follows:

1. Enter the value of bridge voltage
2. Press the Continue key
3. Enter the value of $e_{sum}$ r.m.s. value
4. Continue key
5. Enter the value of $e_{difference}$ r.m.s. value
6. Continue key
7. Enter the value of $R_{AB}$ for the Reynolds Shear stress
8. Continue key.

This program will print out the values of

1. $u'/\bar{U}$, 2. $w'/\bar{U}$ and $\overline{u'w'}/\bar{U}^2$.

## PROGRAM TO COMPUTE RICHARDSON NUMBERS

The temperatures and velocities at the two heights $z_1$ and $z_2$ for the layer whose Richardson number has to be computed is fed into the Wang Computer. The program is given below.

01 - Mark
60 - 0
01 - Stop
Enter the value of Temperature $T_2$
06 - Continue
13 - Store Full (in)
61 - 1
01 - Stop
Enter the value of $T_1$
06 - Continue
50 - Clear Adder (Right)
53 - Subtract
17 - Recall Full (from)
61 - 1
52 - Add
13 - Store Full (in)
62 - 2
01 - Stop
Enter the value of velocity $\bar{U}_2$
06 - Continue
13 - Store Full (in)
63 - 3
01 - Stop
Enter the Velocity $\bar{U}_1$
06 - Continue
54 - Clear Adder (Left)
57 - Subtract
17 - Recall
63 - 3
56 - Add
41 - Enter
66 - 6
75 - .
65 - 5 (Multiply by $\bar{U}_{max}$ if the
62 - 2 velocities entered are in
70 - 8 dimensionless form, $\bar{U}/\bar{U}_{max}$)
46 - Multiply
45 - Square
13 - Store Full (in)

```
64 - 4
63 - 3
62 - 2
75 - .     (acceleration due to gravity)
62 - 2
41 - Enter
63 - 3
60 - 0     ( mean temperature in degrees
60 - 0
75 - .       Absolute)
47 - Divide
13 - Store Full (in)
65 - 5
17 - Recall Full (from)
62 - 2
50 - Clear Adder (Right)
52 - Add
60 - 0
75 - .
60 - 0
60 - 0
60 - 0
62 - 2     (Adiabatic Lapse Rate)
65 - 5
60 - 0     ( in degrees per inch)
65 - 5
52 - Add
41 - Enter
17 - Recall Full (from)
64 - 4
47 - Divide
41 - Enter
17 - Recall Full (from)
65 - 5
46 - Multiply
24 - Write
23 - Special Format
24 - Write
71 - 9       (Carriage Return)
02 - Search
60 - 0
```

This program will print out the Richardson numbers.

# APPENDIX D

## Test Section Calibration Curves

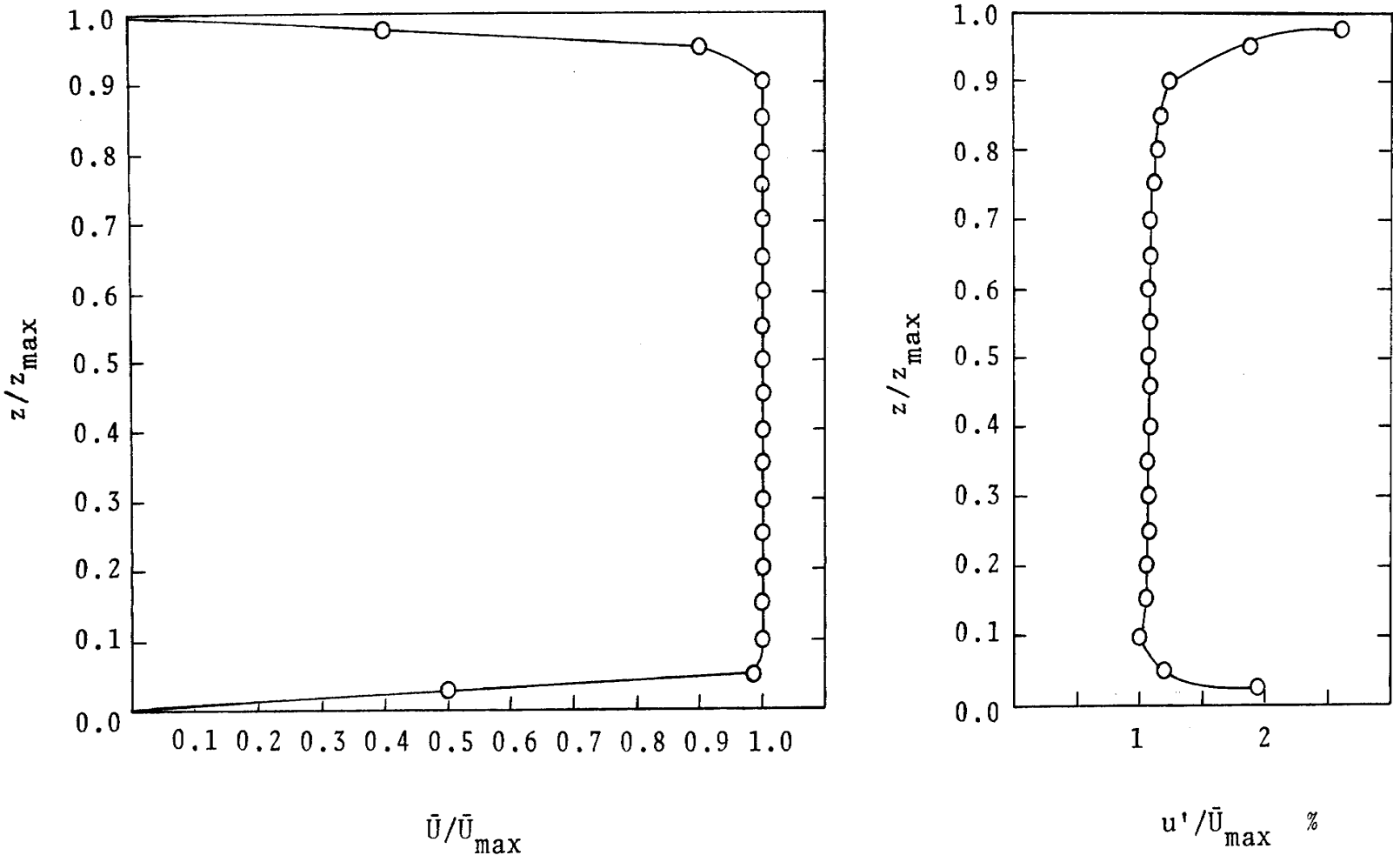


Figure D-1. Velocity and Turbulence Intensity (longitudinal) Profiles at Station 2